Mec1/Tel1-independent role of protein phosphatase 4 in Hop1 assembly to promote meiotic chromosome axis formation in budding yeast

Ke Li[1,2], Miki Shinohara[1,3,4,*]

[1]Institute for Protein Research, Osaka University, Suita, Osaka 565-0871, Japan

[2]Department of Bioscience, Graduate School of Science, Osaka University, Toyonaka, Osaka 560-0043, Japan

[3]Department of Advanced Bioscience, Graduate School of Agriculture, Kindai University, Nara city, Nara 631-8505, Japan

[4]Agricultural Technology and Innovation Research Institute, Kindai University, Nara city, Nara 631-8505, Japan

∗Correspondence:

Miki Shinohara

Department of Advanced Bioscience, Graduate School of Agriculture, Kindai University

3327-204 Nakamachi, Nara, Nara 631-8505, Japan

Phone: +81-742-43-6518

FAX: +81-742-43-8976

E-mail: mikis@nara.kindai.ac.jp

ORCID ID: 0000-0002-7413-8235

Abstract

Dynamic changes in chromosomal structure that occur during meiotic prophase play an important role in the progression of meiosis. Among them, meiosis-specific chromosomal axis-loop structures are important as a scaffold for integrated control between the meiotic recombination reaction and the associated checkpoint system to ensure accurate chromosome segregation. However, the molecular mechanism of the initial step of chromosome axis-loop construction is not well understood. Here, we showed that, in budding yeast, a Tel1/Mec1-related protein phosphatase 4 (PP4) is required to promote the assembly of a chromosomal axis components Hop1 and Red1 onto meiotic chromatin via interaction with Hop1. PP4 did not affect Rec8 assembly. Notably, unlike the previously known function of PP4, this novel function was independent of Tel1/Mec1 kinase functions. The defect in Hop1/Red1 assembly in the absence of PP4 function was not suppressed by Pch2 dysfunction. Since Pch2 is a conserved AAA+ ATPase and facilitates eviction of Hop1 protein from the chromosome axis, suggesting that PP4 is required for the initial step of chromatin loading of Hop1 rather than stabilizing Hop1 on the chromosome axis. These results indicate phosphorylation/dephosphorylation-mediated regulation of Hop1 recruitment onto chromatin during chromosome axis construction before meiotic double-strand break formation.

(194 words)

Introduction

Meiotic recombination is essential for proper segregation of homologous chromosomes during the first meiotic division (meiosis-I) and is initiated by Spo11-dependent programmed meiotic DNA double-strand break (DSB) formation at meiotic recombination hot spots (KEENEY 2001). Meiotic DSB formation and subsequent meiotic recombination require a specific scaffold, an axis-loop structure of chromatin (SHINOHARA *et al.* 2000; BLAT *et al.* 2002; PANIZZA *et al.* 2011). A highly conserved meiotic chromosome axis structure contains core factors Red1, Hop1, and meiosis-specific cohesin complexes, including the meiosis-specific subunit Rec8 in budding yeast (ROCKMILL AND ROEDER 1988; HOLLINGSWORTH AND BYERS 1989; KLEIN *et al.* 1999). After meiotic DSB formation, recombinases Rad51/Dmc1 are recruited to single-stranded DSB ends (BISHOP *et al.* 1992; BISHOP 1994; SHINOHARA *et al.* 1997). The single-stranded DSB ends promote the assembly of Zip-Msh-Mer/synapsis initiation complex (ZMM/SIC) proteins, including the transverse element component Zip1, to construct the synaptonemal complex (SC) and promote crossover (CO) formation (SYM *et al.* 1993; NOVAK *et al.* 2001; BORNER *et al.* 2004; SHINOHARA *et al.* 2008; SHINOHARA *et al.* 2015; DE MUYT *et al.* 2018). In the early leptotene, Zip1 with Zip3 localizes to the centromere and mediates centromere pairing as an initial process to promote chromosome pairing (TSUBOUCHI AND ROEDER 2005; FALK *et al.* 2010).

Hop1 is an axis-associated HORMA-domain protein with multiple roles during meiotic recombination. Hop1 is required for efficient meiotic DSB formation, inter-homolog bias in meiotic recombination, and meiotic prophase checkpoint activation and inactivation (HOLLINGSWORTH *et al.* 1990; SCHWACHA AND KLECKNER 1997; NIU *et al.* 2005; CARBALLO *et al.* 2008; PANIZZA *et al.* 2011; WEST *et al.* 2018). Hop1 together

69 with Red1 promotes DSB formation. Hop1 is phosphorylated by Tel1/Mec1 (yeast
70 ATM/ATR) kinases, which are sensor kinases of DSBs that activate the meiotic
71 prophase checkpoint signaling pathway via Mek1/Mre4 kinase in response to meiotic
72 recombination as well as synapsis defects (NIU *et al.* 2005; BORNER *et al.* 2008). Hop1,
73 Red1, and Mek1/Mre4 form the RHM complex involved in forming a stable axis
74 structure as a scaffold to integrate recombination and the required regulatory
75 responses associated with it. After meiotic DSB repair, Zip1-mediated SC formation
76 and a conserved AAA+ ATPase Pch2 promote Hop1 removal from the synapsed
77 chromosome axis and attenuate the checkpoint signal (BORNER *et al.* 2008). Recently,
78 Pch2 was demonstrated to be involved in the activation as well as the inactivation of
79 meiotic prophase checkpoint through Hop1 (RAINA AND VADER 2020). Thus, Hop1
80 phosphorylation is a key step to complete proper meiotic recombination.
81 Tel1/Mec1 is also required for the integrated meiotic recombination and
82 checkpoint activation. Mec1/Tel1 kinase is involved in intra-chromosomal regulation of
83 the distribution of meiotic DSB formation sites (ANDERSON *et al.* 2015; JOSHI *et al.*
84 2015; CHALLA *et al.* 2019) and signal transduction of the positive/negative feedback
85 loop of meiotic DSB formation through Rec114 phosphorylation (SASANUMA *et al.* 2007;
86 CARBALLO *et al.* 2008; ZHANG *et al.* 2011). In addition Mec1/Tel1 mediates DSB
87 interference as well as CO interference which is required for non-random distribution
88 (ZHANG *et al.* 2011; GARCIA *et al.* 2015; SHINOHARA *et al.* 2019).
89 Protein phosphatase 4 (PP4) is a conserved putative serine/threonine protein
90 phosphatase that functions specifically in response to DNA damage by attenuating the
91 phosphorylation signal by Mec1 and Tel1 during mitosis and meiosis (HOFFMANN *et al.*
92 1994; KEOGH *et al.* 2006; O'NEILL *et al.* 2007; FALK *et al.* 2010; LAI *et al.* 2011;

93 HUSTEDT *et al.* 2015). Mec1/Tel1 phosphorylates many target proteins including Rad53,
94 an ortholog of Chk2 kinase in budding yeast. In the mitotic DNA damage response
95 pathway, PP4 dephosphorylates these targets in the process of recovery from DNA
96 damage-induced signal transduction (O'NEILL *et al.* 2007). Several studies have
97 revealed the meiotic DSB-associated function of PP4 during meiotic recombination
98 (FALK *et al.* 2010; CHUANG *et al.* 2012). During meiosis, centromere pairing is regulated
99 by the balance of phosphorylation and dephosphorylation of Zip1 through Mec1/Tel1
100 kinase and PP4 phosphatase (FALK *et al.* 2010).
101 Here, we focused on the novel function of PP4 which is independent of
102 Mec1/Tel1 function in early prophase-I, especially in a proper meiotic chromosome axis
103 construction via physical interaction with Hop1 protein.
104

105 Results

106 **PP4 activity is required for timely meiotic DSB formation and efficient CO**

107 **formation**

108 Pph3 is a catalytic subunit of the yeast PP4 complex. Pph3 contains several

109 serine/threonine phosphatase motifs (HOFFMANN *et al.* 1994). We constructed a

110 catalytic mutation in the yeast *PPH3* gene by substitution of the conserved histidine

111 residue 112 required for phosphate binding with asparagine (SHI 2009) to generate the

112 *pph3-H112N* mutant (Figure 1A). The mitotic phenotypes of cells with this mutation

113 were analyzed. Pph3 is required for Rad53 dephosphorylation and mitotic DNA

114 damage repair (O'NEILL *et al.* 2007). The *pph3-H112N* mutation did not affect the

115 expression of another PP4 subunit Psy2, with conjugation of a 13-repeated Myc

116 epitope tag (Psy2-13Myc) (Figure S1A). In addition, we analyzed the assembly of

117 Psy2-13Myc on to meiotic chromatin in pachytene cells (Figure 1B). Consistent with a

118 previous study (FALK *et al.* 2010), we detected Psy2-13Myc signals as punctate foci on

119 meiotic chromatin. Importantly, the *pph3-H112N* mutation did not affect the Psy2-

120 13Myc localization. Pph3 and Psy2 form a very stable PP4 complex (O'NEILL *et al.*

121 2007), this suggesting that the catalytic activity of PP4 is not required for its meiotic

122 chromatin localization. Folk et al. reported the meiotic phenotypes of the *pph3*-null

123 (*pph3*Δ) mutant (FALK *et al.* 2010). Therefore, we characterized two *pph3* mutants,

124 *pph3*Δ and *pph3-H112N*, to understand the function of PP4 and its phosphatase

125 activity during meiosis in more detail. First, it was revealed that both *pph3* mutants

126 showed similarly delayed meiosis progression compared to the wild type (Figure S1B).

127 This result was consistent with a previous study on meiosis progression in the *pph3*Δ

128 and *psy2*Δ mutants (FALK *et al.* 2010).

129 To confirm whether the delayed meiosis progression in *pph3* mutants is
130 caused by meiotic recombination defects, we analyzed programmed meiotic DSB
131 formation as an initial event of meiotic recombination by Southern blotting at the *HIS4-*
132 *LEU2* hot spot in chromosome III in the *pph3* mutants, although meiotic crossover
133 formation defects in *pph3*Δ have already been reported (FALK *et al.* 2010). The *HIS4-*
134 *LEU2* hot spot is a well-analyzed artificial meiotic DSB hotspot that includes two known
135 sites, DSB I and II (Figure 1C). We detected and quantified DSB I and showed its
136 frequencies at each time point after meiosis entry (Figure 1D). Meiotic DSBs became
137 detectable 3 h after meiosis entry, and showed a peak at 4 h, and disappeared by 6 h
138 in the wild type (Figure 1D). On the other hand, both *pph3-H112N* and *pph3*Δ showed
139 an approximately 1 h delay in DSB formation compared to the wild type at the time
140 when the DSB reached half of the peak height (11%; Figure 1D, dashed line). In
141 addition, the *pph3* mutants showed an accumulation of meiotic DSBs with hyper-
142 resected ends until 6 h after meiosis entry, resulting in an approximately 3 h delay in
143 DSB disappearance (Figure 1D). These observations indicated the necessity of PP4
144 phosphatase activity for efficient DSB formation and turnover. PP4 is a Mec1/Tel1-
145 related protein phosphatase. Previous studies revealed that PP4 is required for
146 centromere pairing through Zip1 dephosphorylation for Mec1-mediated
147 phosphorylation at S75, or dephosphorylation of many other Mec1/Tel1 targets during
148 meiosis (KEOGH *et al.* 2006; FALK *et al.* 2010; HUSTEDT *et al.* 2015). Thus, we
149 constructed mitotic cyclin *CLB2* promoter-driven *MEC1* (p*CLB2-MEC1*) *tel1*Δ allele to
150 determine the effect of Mec1 and Tel1 on delayed DSB formation and/or turnover in the
151 *pph3* mutants. p*CLB2* induces mitosis-specific gene expression. Thus, p*CLB2-MEC1*
152 causes meiosis-specific shutdown of *MEC1* transcription (LEE AND AMON 2003). The

153 p*CLB2-MEC1 tel1*Δ cells showed a reduced level of steady-state meiotic DSB
154 formation (7.7 ± 1.9% of total DNA) compared to that in the wild type (22.7 ± 3.1%).
155 p*CLB2-MEC1 tel1*Δ and p*CLB2-MEC1 tel1*Δ *pph3*Δ triple mutants showed more
156 severe reduction of DSB formation (5.3 ± 0.45% and 7.7 ± 3.2%, respectively; Figure
157 1D, graph). At later time points, in contrast to the *pph3* mutants, the p*CLB2-MEC1*
158 *tel1*Δ and p*CLB2-MEC1 tel1*Δ *pph3*Δ mutants showed the timely disappearance of
159 meiotic DSBs by 6 h in meiosis (Figure 1D). These findings suggested that the
160 accumulation of DSBs and the resulting delay in DSB repair, which was observed in
161 the *pph3* mutants at later time points (at 5–6 h) was dependent on Mec1/Tel1 (Figure
162 1E). In contrast, in the initiation of DSB formation, the p*CLB2-MEC1 tel1*Δ *pph3*Δ triple
163 mutant showed a peak at 4 h, whereas the p*CLB2-MEC1 tel1*Δ double mutant peaked
164 between 3 and 4 h after onset of meiosis entry (Figure 1E, graph). Since a delay in
165 meiotic DSB formation in the absence of Tel1/Mec1 activity was observed, the delayed
166 DSB formation caused by pph3 mutations appeared to be independent of Mec1/Tel1.
167 Next, we analyzed hetero-duplex (HD) formation using Southern blot to
168 analyze meiotic inter-homolog recombination products by using heteroallelic restriction
169 enzyme sites *Mlu*I and *Bam*HI located near the DSB I site and polymorphic *Xho*I sites
170 around the *HIS4-LEU2* hot spot (Figure 1C) (STORLAZZI *et al.* 1996). Corresponding to
171 the delayed meiotic DSB appearance and disappearance at the hot spot, the formation
172 of both HDs corresponding to intermediates for crossover (CO) and non-crossover
173 (NCO) were delayed by 3 h in the *pph3* mutants relative to that in the wild type (Figure
174 1E). In addition, an increase of NCO intermediates (HD1 and 4) at 8 h and a slight
175 reduction of CO intermediates (HD2 and 3) compared to wild type were observed not

176 only in the *pph3*Δ, as reported previously (FALK *et al.* 2010), but also in the *pph3-*
177 *H112N* mutant (Figure 1E).
178 After DSB end resection, meiotic DSBs are recognized by recombinases
179 Rad51 and Dmc1 to facilitate strand exchange for the formation of COs and NCOs.
180 The cytological analysis revealed that Rad51 appear transiently as punctate foci on
181 meiotic chromatin structure in the wild type (SHINOHARA *et al.* 2000). Thus, we next
182 examined the kinetics of Rad51 assembly and disassembly in the *pph3* mutants using
183 cytological analysis (Figure 1F). In the *pph3* mutants there was a 1 h delay in the
184 Rad51 assembly compared to the wild type. In addition, accumulation of Rad51 foci
185 was evident by 5 h after meiotic entry (Supplemental Figure 1C). On the other hand,
186 the number of Rad51 foci per nucleus at an early time point (3 h) in the *pph3*Δ and
187 *pph3-H112N* mutants was significantly lower than that in the wild type (64 ± 2.7, 56 ±
188 2.7, and 49 ± 3.3, respectively; Figure 1F). This also indicated the involvement of PP4,
189 as well as its phosphatase activity, for efficient DSB formation. In the disassembly
190 phase of Rad51 foci, a significant reduction in the number of Rad51 foci per nucleus
191 was observed in the wild type. However, continuous accumulation of Rad51 foci was
192 observed in the *pph3* mutants corresponding to inefficient meiotic DSB repair.
193
194 **PP4 is involved in efficient Hop1 assembly onto chromatin in a Mec1/Tel1-**
195 **independent manner**
196 Hop1 is a meiosis-specific phosphorylation target of Mec1 and Tel1, and PP4 is
197 involved in the dephosphorylation of these targets (CARBALLO *et al.* 2008; FALK *et al.*
198 2010). Furthermore, Hop1 is a HORMA-domain protein and a component of the axis
199 structure as a complex with Red1 to form the SC. Hop1 is essential for partner choice

200 of meiotic recombination (known as inter-homolog bias) and for efficient DSB formation
201 (HOLLINGSWORTH *et al.* 1990; NIU *et al.* 2005; PANIZZA *et al.* 2011; SUBRAMANIAN *et al.*
202 2016). Since it was observed (Figure 1C and D) that PP4 is required for efficient
203 initiation of meiotic DSB formation, we analyzed the kinetics of Hop1 assembly during
204 meiotic prophase-I (Figure 2A). In wild type Hop1, assembly began 2 h after the onset
205 of meiosis, corresponding to leptotene, and occurred prior to DSB formation.
206 We also analyzed the localization of Hop1 and Hop1 phosphorylated at
207 threonine 318 (Hop1-pT318) on meiotic chromatin. Hop1 phosphorylation is dependent
208 on Mec1/Tel1 kinase activation by Spo11-induced meiotic DSB formation (CARBALLO *et*
209 *al.* 2008). Hop1-pT318 has been observed as punctate foci at the end of short patches
210 of Hop1 signal in the wild type (CARBALLO *et al.* 2008) (Figure 2A and B). In the wild
211 type, 50% of the cells displayed Hop1 foci 2 h after meiosis entry, but low levels of
212 Hop1-pT318 were observed at the same time. Hop1-pT318 foci began to appear after
213 3 h (Figure 2A and B). Hop1-pT318 focus formation requires single-stranded region at
214 meiotic DSB ends (IWASAKI *et al.* 2016). The time lag of approximately 2 h that was
215 evident between the Hop1 loading and the Hop1-pT318 appearance in the present
216 study indicated that Hop1 assembly occurs prior to the DSB formation and/or DSB-end
217 resection in wild type. In the *pph3* mutants, Hop1 assembly was rarely seen at 2 h
218 compared to the wild type. After 2 h, Hop1 staining gradually increased and reached
219 the wild-type level frequency (80%) at 5 h. Notably, pT318 staining appeared at almost
220 the same time (3 h) as the appearance of Hop1 foci (Figure 2A and B) and then
221 gradually increased, similar to Hop1. Hop1 loading seemed to be the rate-limiting factor
222 for Hop1 phosphorylation. These results showed that Pph3 and its activity can promote

223 the efficient loading of Hop1 on chromosomes. We confirmed that this was not due to
224 delayed expression of Hop1 in the mutant (see Figure 2C).
225 Next, we examined the effect of Mec1 and Tel1 on Hop1 assembly in the
226 *pph3*Δ mutant. While the p*CLB2-MEC1 tel1*Δ mutant cells did not show any defects in
227 the Hop1 assembly, the p*CLB2-MEC1 tel1*Δ *pph3*Δ mutant displayed delayed Hop1
228 assembly, similar to the *pph3* mutants (Figure 2A and B). In contrast, very few Hop1-
229 pT318 foci were observed in the p*CLB2-MEC1 tel1*Δ mutation background.
230 Next, we analyzed the phosphorylation status of target proteins of PP4 during
231 meiosis using western blot. PP4 is known to be involved in dephosphorylation of
232 phosphorylated S129 of histone H2A (γH2A) after DNA damage in vegetative growth
233 cells (KEOGH *et al.* 2006), and in Hop1-pT318 during meiosis (CHUANG *et al.* 2012).
234 Thus, we first confirmed that γH2A signal accumulated in the *pph3* mutants during
235 meiosis in a Mec1/Tel1 dependent manner, similar to mitotic cells, with markedly
236 reduced γH2A signals in the p*CLB2-MEC1 tel1*Δ *pph3*Δ mutant (Figure 2C). Moreover,
237 accumulation of Hop1-pT318 signal was also observed until 8 h in the *pph3*Δ mutant.
238 This phosphorylation was dependent on Mec1/Tel1 (Figure 2C). Although Hop1 protein
239 expression was detectable from 2 h after meiosis entry in both wild type and *pph3*
240 mutants, initiation of Hop1 phosphorylation at T318 was delayed by 1 h in the *pph3*
241 mutants compared to the wild type to reach maximum levels. Notably, despite the
242 timely expression of Hop1 protein in the *pph3* mutants (Figure 2D), the appearance of
243 Hop1 foci on meiotic nuclear spread was significantly delayed in the *pph3* mutants
244 (Figure 2A). This result suggested that PP4 might not be involved in Hop1 expression,
245 but rather acted to promotes Hop1 loading onto chromatin. Moreover, the expression
246 kinetics of Hop1 protein were also normal in the p*CLB2-MEC1 tel1*Δ or p*CLB2-MEC1*

247 *tel1*Δ *pph3*Δ mutants. In contrast to the γH2A phosphorylation, residual Hop1-pT318
248 signal was not detected in the p*CLB2-MEC1 tel1*Δ background, consistent with a
249 previous report showing that Hop1 phosphorylation largely depends on Mec1 and Tel1
250 activities (CARBALLO *et al.* 2008). Overall, the findings indicate a defect in Hop1
251 assembly on chromatin, even though a sufficient amount of Hop1 protein is expressed.
252
253 **PP4 is involved in meiotic chromosome axes formation**
254 Next, we examined the Red1 and Rec8 meiotic chromosome axis components
255 (ROCKMILL AND ROEDER 1988; KLEIN *et al.* 1999). Red1 forms a complex with Hop1
256 (NIU *et al.* 2005) and Rec8 is a component of the meiosis-specific sister chromatid
257 cohesin complex. Both proteins are required for the proper formation of axial elements
258 in meiosis and a highly-ordered specific chromosome structure, termed the
259 synaptonemal complex (SC) (KLEIN *et al.* 1999). Red1 and Rec8 are recruited to the
260 chromatin independent of each other (SUN *et al.* 2015). We examined Red1 and Rec8
261 staining of the meiotic chromatin (Figure 3A). In the wild type, Red1 and Rec8
262 colocalized with each other and formed linear structures along the 4′,6-diamidino-2-
263 phenylindole (DAPI) nuclear signal on meiotic chromatin 3 h after meiosis entry. In
264 contrast, in the *pph3* mutants, Red1 and Rec8 were observed as many fine signals
265 throughout the chromatin spreads. The number of Rec8 signals was clearly higher than
266 that of Red1. Time course experiments revealed the significant delay in the assembly
267 of Red1 protein in the *pph3* mutants, similar to the assembly of Hop1 shown in Figure
268 2A and 2B. In contrast, the timing of Rec8 assembly, despite of its unique structure,
269 was not affected in the presence or absence of Pph3 activity (Figure 3B). In addition, a
270 delay in the disassembly of both Red1 and Rec8 was observed in the *pph3* mutants.

271 Next, we analyzed Red1 and Rec8 protein expression during meiosis using
272 western blot (Figure 3C). Rec8 phosphorylation via Dbf4-dependent kinase (DDK) and
273 polo-like kinase 1 (PLK1) is associated with cleavage-independent cohesion release
274 from chromatin during late prophase-I (CHALLA *et al.* 2019). While the expression of
275 Rec8 occurred at almost the same time in the *pph3* mutants as that in the wild type, the
276 phosphorylation of Rec8 was delayed in the *pph3* mutants compared to that in the wild
277 type. Corresponding to the delayed phosphorylation of Rec8, Rec8 cleavage that
278 occurs during the meiotic divisions was also delayed in the *pph3* mutants. These
279 results were consistent with the delayed meiosis progression of meiosis in *pph3*
280 mutants (Figure S1). In addition, Red1 protein expression was quite normal in the *pph3*
281 mutants (Figure 3C). These results suggest that PP4 promotes Hop1-Red1 loading but
282 not Rec8-cohesin, which is required for the construction of a proper axis structure.
283
284 **PP4 physically interacts with Hop1 protein**
285 We next examined the physical interaction between the Hop1-Red1 and PP4 using a
286 co-immunoprecipitation assay (Figure 4A). Psy2-13Myc protein was precipitated using
287 anti-Myc antibody in meiotic cell extracts of *PSY2-13MYC* derivative *PPH3* (wild type)
288 cells. The Hop1 signal was detected in the precipitate from the cells at 2 to 6 h during
289 meiosis, indicating the interaction of Pys2 with Hop1. The Hop1 signal was also
290 detected in the precipitates of *pph3-H112N* mutant cells, indicating that the interaction
291 did not involve the phosphatase activity of PP4. However, the Hop1 signal was weaker
292 at 4 h than that in the *PPH3* background and was undetectable at 6 h in meiosis. This
293 might be caused by reduced amounts of the Psy2-13Myc protein signal in the
294 precipitates. However, the total amount of Psy2-13Myc protein in the *pph3-H112N*

295 mutant whole cell extracts of the *pph3-H112N* mutant from trichloroacetic acid-fixed
296 cells was indistinguishable from that in wild type-cells (Supplemental Figure 1A). A
297 mutation in *PPH3* affected the interaction between Hop1 and Psy2-13Myc, indicating
298 the interaction between Hop1 and the PP4 complex, rather than Psy2 alone (as an
299 independent complex).

300 Since Hop1-PP4 physical interaction was detected, we analyzed other axis
301 components Red1 and Rec8 proteins in the precipitates using western blot. After
302 immunoprecipitation in *PSY2-13MYC* cell extracts, as described above, the Hop1
303 protein signal was observed at 2 and 4 h after meiosis entry. However, the signal was
304 not evident at 6 h, even though Hop1 protein was expressed in the extract. In contrast,
305 Red1 and Rec8 were not observed in the precipitates, even though both proteins were
306 present in whole cell extracts (WCE). The findings indicates that PP4 can interacts with
307 Hop1 mainly, but not Red1 or Rec8. Given that Hop1 binds to Red1 as a complex (NIU
308 *et al.* 2005), there might be two distinct populations of Hop1, Hop1-PP4 and Hop1-
309 Red1.

310

311 **Defective Hop1 assembly onto chromosome axes in the *pch2*Δ background in**
312 **the *pph3* mutant**

313 Pch2 is a AAA+ ATPase that removes Hop1 protein from meiotic chromosome axes to
314 stabilize the transverse element Zip1 during formation of the SC structure (CHEN *et al.*
315 2014). Pch2 is also involved in a PP4-independent Hop1 dephosphorylation (CHEN *et*
316 *al.* 2014). Since we observed a defect in Hop1 assembly and delayed phosphorylation
317 of Hop1 in the *pph3* mutants, we analyzed the effects of the *pph3* mutations in the

318 Hop1 assembly on the meiotic chromosome axis in the *pch2*Δ background, which
319 features the over-loading of Hop1.
320 First, spore viability and distribution of viable spores were analyzed in the
321 *pph3*Δ *pch2*Δ double mutant by using tetrad analysis. Spore viability in the wild type,
322 *pph3*Δ, and *pch2*Δ was 97%, 88%, and 91%, respectively. Both *pph3*Δ and *pch2*Δ had
323 slightly reduced spore viability, but there was no significant bias in the distribution of
324 viable spores in asci, as reported previously (SAN-SEGUNDO AND ROEDER 1999; FALK *et*
325 *al.* 2010). In contrast, the pore viability of the *pph3*Δ *pch2*Δ double mutant was only
326 25%, with distributions of 0-, 2-, and 4-viable spores. This vias was indicative of the
327 non-disjunction of homologous chromosomes in the first division of meiosis.
328 In Hop1 and Hop1-pT318 assembly/disassembly kinetics, Hop1-pT318
329 assembly was delayed in the *pch2*Δ mutant, consistent with a delayed meiotic DSB
330 formation (FARMER *et al.* 2012). This delay was similar to that in the *pph3*Δ and the
331 *pph3*Δ *pch2*Δ double mutant (Figure 4D and E), indicating the absence of additive
332 defects to *pph3*Δ in Hop1 assembly/disassembly in the *pch2*Δ mutation. The findings
333 suggest that Pch2 and PP4 function in the same pathway in Hop1
334 assembly/disassembly.
335 Next, we examined the effect of the *pch2*Δ mutation on Hop1 localization by
336 using cytological analysis. As indicated previously (IWASAKI *et al.* 2016) and in Figure
337 2A, Hop1-pT318 foci were observed as punctate foci in the wild type and were affected
338 in the *pph3*Δ in early prophase-I (approximately 3 h in meiosis) (Figure 4E). In the
339 *pch2*Δ mutant, Hop1 aggregates colocalized with Hop1-pT318 signals. Similar
340 aggregates were also observed in the *pph3*Δ *pch2*Δ double mutant at an early time
341 point.

342 Notably, at the later time point (6 h during meiosis), Hop1-pT318 signals were
343 observed as a beaded chain on the fully elongated Hop1 signal on meiotic
344 chromosomes in the *pch2*Δ mutant cells (Figure 4E). In the *pph3*Δ *pch2*Δ double
345 mutant, some Hop1 signals were observed as foci of dots and some colocalized with
346 the Hop1-pT318 signal, similar to that in *pph3*Δ. These observations were evidence of
347 the upstream location of the *pph3*Δ mutation relative to the *pch2*Δ mutation in Hop1
348 localization process. This further suggests that PP4 may function in the promotion of
349 Hop1 assembly onto the meiotic chromatin to construct the chromosome axis before
350 Pch2 function in unloading of Hop1 from the chromosome axis. In contrast, in the
351 *pph3*Δ *pch2*Δ double mutant, some Hop1-pT318 signals were observed as beaded
352 chain on fully elongated Hop1. This indicates that the *pch2*Δ mutation stabilized Hop1
353 protein in the *pph3*Δ on some chromosome axis, but not on others. Therefore, there
354 could be other pathways that promote Hop1 assembly in the absence of PP4.
355
356 **Multiple pathways to promote Hop1 assembly**
357 On the meiotic chromosome axes, Hop1 is dynamic and is removed from
358 chromosomes through Pch2 activity. Finally, Hop1 is replaced by the transverse
359 element component Zip1 in the pachytene (BORNER *et al.* 2008). Given these facts, we
360 examined Zip1 localization in the *pph3*Δ *pch2*Δ double mutant. In wild type cells, as
361 previously reported, Zip1 was observed as dotty foci in the leptotene (2 h) and Zip1
362 begins to elongate after DSB-end resection in the zygotene, followed by the extension
363 of Zip1 throughout each chromosome in the pachytene (SYM *et al.* 1993; STORLAZZI *et*
364 *al.* 1996; SHINOHARA *et al.* 2015). Significant delays in both the appearance of dotty
365 Zip1 signals and the elongation of Zip1 were evident for *pph3*Δ (Figure 5A), as

366 reported previously (FALK *et al.* 2010). The *pch2*Δ mutant showed a delay in the Zip1
367 elongation and also dissociation from the chromosomes after full elongation. However,
368 the elongated Zip1 became the major population at 5 h after meiosis. In the *pph3*Δ
369 *pch2*Δ double mutant, after the delayed appearance of dotty Zip1 signals, similar to
370 *pph3*Δ (2 to 3 h), compromised elongation of Zip1 was observed. Complementary
371 localization of Zip1 and Hop1 on chromosomes from the zygotene to the pachytene
372 was observed in the wild type. A similar localization was observed in the *pph3*Δ mutant.
373 In contrast, *pch2*Δ mutant cells showed uniform colocalization of Zip1 and Hop1
374 (Figure 5B), as previously reported (BORNER *et al.* 2008). *Saccharomyces cerevisiae*
375 haploid cells have 16 chromosomes. Theoretically, 16 bivalents should be observed in
376 the pachytene stage: however, the number of linear Zip1 signals per cell was 12 ± 2.7
377 (mean ± 95% confidence interval) in the *pch2*Δ. The number was significantly reduced
378 in the *pph3*Δ *pch2*Δ double mutant in 68% of *pch2*Δ (8.2 ± 2.6) (Figure 5B and C).
379 While several elongated Zip1 signal colocalized with Hop1 in *pph3*Δ *pch2*Δ, Hop1-Zip1
380 free DAPI signal was also often observed in *pph3*Δ *pch2*Δ (Figure 5B). Next, we
381 compared the length of Zip1-Hop1 positive signals in *pch2*Δ with in *pph3*Δ *pch2*Δ to
382 determine whether there is chromosome size bias in the residual elongation of Zip1-
383 Hop1 observed in *pph3*Δ *pch2*Δ. No significant difference was evident (P = 0.19,
384 Figure 5D).

385 Since the *pph3*Δ mutation showed a chromosome-dependent effect in Hop1-
386 Zip1 elongation in the *pch2*Δ mutant background, we analyzed Rec8 and Red1
387 localization, as other axis components, to determine the status of the Hop1-Zip1 free
388 region observed in the *pph3*Δ *pch2*Δ double mutant. Unlike the Hop1 protein on the
389 axes, Red1 is not removed from the axis by Pch2. Rec8 is recruited to chromatin

390 independent of Hop1-Red1 (SUN *et al.* 2015). Furthermore, the Rec8 focus formation
391 was not affected in the *pph3* mutants (Figure 3A). In the *pch2*Δ mutant cell, Rec8 and
392 Red1 obviously colocalized on the chromosome axes (Figure 5E). On the other hand,
393 in the *pph3*Δ *pch2*Δ double mutant, Rec8 and Red1 were colocalized only on the
394 synapsed chromosome axes, and many of the Rec8 were observed as foci located in
395 the Red1 free region. This indicates the possibility that 68% of the chromosomes axes
396 with linearized Hop1 in the *pph3*Δ *pch2*Δ harbored a defect in the Pch2 sensitive step
397 following Hop1 loading, while the defect in other axes was prior to Hop1 assembly.
398
399 **Delayed meiosis progression in the *pph3*Δ occurs independent of Pch2**
400 Hop1 is an adaptor of meiosis-specific prophase checkpoint. Hop1
401 phosphorylation is affected in the *pch2*Δ mutant (LO *et al.* 2014) and Mec1/Tel1-
402 dependent phosphorylation of Hop1 affects Hop1 activity (CARBALLO *et al.* 2008). In the
403 wild type, Hop1 phosphorylation was detectable at 3 h during meiosis, continued until 5
404 h, and then disappeared (Figure 5F). The timing of Hop1-pT318 disappearance
405 matched the timing of the initiation of meiosis-I (Figure 5G). This was also observed
406 with *pph3*Δ mutant cells, in which the Hop1-pT318 signal disappeared at 8 h with the
407 simultaneous appearance of post-meiotic cells. In *pch2*Δ mutant cells, consistent with
408 previous findings, Hop1 protein was accumulated until 10 h and Hop1 phosphorylation
409 was compromised. On the other hand, in the *pph3*Δ *pch2*Δ double mutant, Hop1
410 protein accumulated until 10 h and Hop1-pT318 signal also accumulated until 8 h and
411 then disappeared. Notably, corresponding to the delayed disappearance of the Hop1-
412 pT318 signal, the *pph3*Δ *pch2*Δ double mutant showed a severe delay in meiosis
413 progression (Figure 5E and F). The *pch2*Δ mutation can suppress pachytene arrest in

414 the *zip1* mutant (SAN-SEGUNDO AND ROEDER 1999; BORNER *et al.* 2008). Since the

415 *pch2*Δ mutation cannot suppress the delayed progression of meiosis in the *pph3*Δ

416 mutant, this delay in the *pph3*Δ would be caused by a different mechanism from that in

417 the *zmm* mutant.

418

419

420 **Discussion**

421

422 During meiotic recombination, the chromosome axis is an essential scaffold. Some
423 components, including Mer2 and Rec8, are associated with pre-meiotic DNA
424 replication. On the other hand, the molecular mechanism underlying the formation of a
425 highly organized chromosomal axis structure, especially, the initial step of Hop1
426 recruitment onto meiotic chromatin, is not well understood. The results of the present
427 study support the suggestions that PP4 may function in Hop1 recruitment onto
428 chromatin in the initiation step of chromosome axis formation in early meiotic
429 prophase-I and that PP4 promotes Hop1 recruitment.

430

431 **PP4 is involved in Hop1 assembly independent from Tel1/Mec1 kinase activity**

432 During the formation of the meiotic SC structure, PP4 is required for centromere-
433 mediated chromosome pairing through Zip1 phosphorylation in a Mec1/Tel1-dependent
434 manner (FALK *et al.* 2010). We also observed reduced dotty Zip1 signal, which is
435 known to localize to the centromere (TSUBOUCHI AND ROEDER 2005). The reduction
436 was not suppressed even in the *pch2*Δ background (Figure 5A). Both *pph3* mutants,
437 *pph3*Δ and *pph3-H112N,* displayed significant delays in Hop1 assembly onto chromatin,
438 but this delay was Tel1/Mec1-independent (Figure 2A and B). Therefore, this delay in
439 Hop1 assembly would not be caused by compromised centromere pairing. In *pph3*
440 mutants, the appearance of γH2A, which is phosphorylated by Mec1/Tel1 kinase in
441 response to programmed meiotic DSBs, was observed at the same time as that in wild
442 type. The Hop1 phosphorylation (Hop1-pT318) by Tel1/Mec1 was delayed as well. This
443 result supports the idea that delayed Hop1 phosphorylation is caused by the delayed

444 assembly of Hop1 onto the axes. Hop1 is one of the rate-determining factors that
445 promotes meiotic DSB formation (PANIZZA *et al.* 2011). In addition, we revealed the
446 physical interaction between the Hop1 and PP4 components also in the *pph3-H112N*,
447 a catalytic mutation, and Hop1 protein in the precipitates was not always
448 phosphorylated (Figure 4A and B). This findings suggest that the Hop1-PP4 interaction
449 might not occur only for enzymatic activity, but may also regulate Hop1 assembly.
450 There is still another possibility that Hop1 localization on the chromosome
451 axes in the absence of PP4 is unstable and is rapidly removed from the axes. To
452 assess this, we examined Hop1 localization in the absence of Pch2. Proper Hop1
453 assembly did not occur in 32% of the chromosomes in each nucleus of *pph3*Δ cells.
454 This strongly suggests that PP4 is involved in the assembly phase of Hop1 and not in
455 the stabilization of Hop1 on the chromosome axes. Conversely, 68% of chromosomes
456 in the same nucleus displayed stable Hop1 assembly by *pch2*Δ, even in *pph3*Δ. These
457 observations indicate that there are multiple pathways other than the PP4 that promote
458 Hop1 assembly.
459
460 **What is the molecular mechanism to promote Hop1 assembly?**
461 The molecular mechanism by which PP4 promotes Hop1 assembly through physical
462 interactions is unknown. Hop1 is a HORMA domain protein. The dynamics of C-
463 terminal "closure-motif" may be important for the chromosome axis assembly and
464 disassembly through Red1 interaction. In addition, substitution of K593 of Hop1 with
465 alanine (*hop1-K593A*) results in severe defects in the Red1 interaction (WEST *et al.*
466 2018). We performed phospho-proteomics analysis in extracts from yeast cells
467 arrested in meiotic prophase-I. The finding revealed the phosphorylation of S595 of

468 Hop1 during meiosis, possibly by Mek1/Mre4 kinase (Shinohara M., unpublished
469 result). We previously analyzed Hop1 assembly onto chromatin in the
470 unphosphorylated mutation background of *hop1-S595L*. Normal Hop1 assembly was
471 observed in the *hop1-S595L* mutant.

472 In addition, a delay in Hop1 assembly in the *pph3*Δ mutant was also observed
473 in the p*CLB2-MEC1 tel1*Δ background, and Pph3 catalytic activity was required for the
474 timely assembly of Hop1 (Figure 2A and B). These observations indicate that
475 dephosphorylation of the target protein through PP4 is required for efficient assembly
476 of Hop1, that Tel1/Mec1 is dispensable from the phosphorylation of the target(s), and
477 that this phosphorylation may occur before meiotic DSB formation (Figure 6). Hop1
478 may be the most probable target for dephosphorylation by PP4. On the other hand, the
479 candidate protein kinase(s) that regulate Hop1 assembly are DDK and/or CDK.
480 However, the ATP analog sensitive *cdc7* allele (*cdc7-as3*) reportedly showed normal
481 Hop1 expression but no Hop1 phosphorylation in the presence of an ATP analog (WAN
482 *et al.* 2006). The yeast Cdc28, a component of CDK, focus formation on meiotic
483 chromatin are dependent on Hop1, Red1 and Rec8, but not on Mek1/Mre4. The analog
484 sensitive allele *cdc28-as1* reportedly displayed compromised Rad51 focus formation
485 and severe defects in Zip1 elongation, but did not affect Red1 loading in the presence
486 of an ATP analog (ZHU *et al.* 2010). These findings indicate that CDK and DDK
487 functions are associated with Hop1 function. However, direct phosphorylation of Hop1
488 by CDK and/or DDK has not been reported. There are two predicted CDK
489 phosphorylation motifs (S/T-P) in Hop1: S494 and S531 (ZHU *et al.* 2010). The
490 presence of sequential phosphorylation by CDK followed by DDK in the sequence of
491 serine/threonine residues in addition to the CDK phosphorylation motif has been

492 described for related target proteins such as Mer2 (WAN *et al.* 2006) and Mps3 (RAO *et*
493 *al.* 2020), and the S494 of Hop1 overlaps this motif (T-S-^{494}S-P).
494
495 **PP4 has an independent role from ZMM/SIC components in the prophase**
496 **checkpoint**
497 Pch2 activates the meiotic prophase checkpoint when meiotic DSB repair or
498 chromosome synapsis is compromised in *zip1*, *zip2*, or *dmc1* mutant cells (SAN-
499 SEGUNDO AND ROEDER 1999; BORNER *et al.* 2008). It has been reported that the PP4
500 mutant shows a *zmm* mutant-like phenotype in meiotic recombination, NCO/CO ratio
501 aberration, temperature-sensitive meiosis progression, CO formation, and
502 compromised CO interference (BORNER *et al.* 2004; FALK *et al.* 2010). In addition,
503 defective CO formation in *pph3*Δ is epistatic to *msh4*Δ (FALK *et al.* 2010). We also
504 observed compromised CO and elevated NCO formation through HD analysis (Figure
505 1C). These are often observed in *zmm* mutants (SHINOHARA *et al.* 2008). *pch2*Δ could
506 not suppress the delayed meiosis progression of the *pph3*Δ mutant. These findings
507 suggest that delayed meiosis progression is caused by a different mechanism from that
508 of *zmm* or *dmc1* mutants. Recently, it was reported that Pch2 in collaboration with
509 Hop1 mediates the meiotic prophase checkpoint (RAINA AND VADER 2020). In the *pph3*
510 mutants, compromised synapsis as well as inefficient meiotic recombination easily
511 activated the meiotic prophase checkpoint because of enhanced Mec1/Tel1 signaling,
512 but the checkpoint signal could not be restored even in the absence of Pch2. This
513 could be caused by insufficient Hop1 loading on the chromosome axis or accumulation
514 of unbound inactive form of Hop1 protein (Figure 6).
515

516 **Materials and Methods**

517 **Yeast strains and media**

518 All the yeast strains and their genotypes are listed in Supplemental table 1. We used
519 isogenic *S. cerevisiae* SK1 background NKY1551 derivatives (STORLAZZI *et al.* 1996).
520 *PPH3-13MYC* was constructed using a PCR-based tagging method (BAHLER *et al.*
521 1998). *pph3-H112N* was constructed vis two-step gene replacement. YPAD (1% yeast
522 extract, 2% Bacto peptone, 0.01% adenine, 2% glucose), SPM (0.3% potassium
523 acetate, 0.03% raffinose), and DISS plates (YPAD medium containing 2.4% Bacto
524 Agar) were used.

525

526 **Yeast meiosis time course**

527 The experiments were performed as described previously (SHINOHARA *et al.* 2003).
528 Meiosis progression was analyzed by counting the number of nuclei in each ascus at
529 each time point. Nuclei were visualized by staining with 4', 6-diamidino-2-phenylindole,
530 dihydrochloride (DAPI) and observed under an epifluorescence microscope
531 (AxioSkop2, Carl Zeiss). More than 100 nuclei were analyzed at each time point.

532

533 **Cytological analysis**

534 Immunostaining of yeast meiotic nuclear spreads was performed as previously
535 described (SHINOHARA *et al.* 2015). Stained samples were observed under
536 epifluorescence using the Axioskop 2 microscope equipped with light-emitting diode
537 fluorescence light sources (X-Cite; Excelitas Technologies) and a 100× objective
538 (AxioPlan, NA1.4, Carl Zeiss). Images were captured with a CCD camera (Retiga;
539 Qimaging) and processed using iVision (BioVision Technologies) and Photoshop

540 (Adobe). The antibodies used in these assays were anti-Hop1 (IWASAKI *et al.* 2016)
541 (guinea pig, 1:500) and anti-Hop1-pT318(IWASAKI *et al.* 2016) (rabbit, 1:500), anti-Red1
542 (chicken, 1:500) (SHINOHARA *et al.* 2008) and anti-Rec8 (rabbit, 1:1000) (ZHU *et al.*
543 2010). Nuclei containing more than five foci were counted as focus-positive.
544
545 **Southern blot to detect meiotic DSBs and recombination intermediates**
546 Genomic DNAs prepared from yeast meiosis time course experiments were digested
547 with *Mlu*I, *Bam*HI, and *Xho*I for heteroduplexes (HDs), and *Pst*I for meiotic DSBs.
548 Probes for Southern blotting were Probe 155 for HD and Probe 291 for DSB detection
549 (STORLAZZI *et al.* 1996; SHINOHARA AND SHINOHARA 2013). They were labeled with α-
550 ^{32}P- dATP (NEG512H, PerkinElmer) using the random primer method (Random Primer
551 6, NEB S1230S, Klenow fragment (3'-5' exo-, M0210) and visualized by using
552 FLA7000 (Cytiva). The visualized signals were analyzed by using Image Quant TL
553 software (Cytiva).
554
555 **Western blotting**
556 Western blotting was performed as described previously (SHINOHARA *et al.* 2015).
557 Meiotic yeast cell extracts were prepared by cell disruption using a Multi-Beads Shocker
558 (YASUIKIKAI) after trichloroacetic acid treatment. The primary antibody signal was
559 visualized using Alexa Fluor 680–labeled secondary antibodies (Thermo Fisher
560 Scientific) or IRDye 800CW–labeled secondary antibodies (LI-COR Biosciences) using
561 an Odyssey infrared imaging system (LI-COR Biosciences). The primary antibodies
562 used in these assays were anti-γH2A (anti-γH2A, AF2288, R&D Systems, 1:1000),
563 anti-Myc (MC045, Nacalai Tesque, 1/1000), anti-Hop1 (guinea pig, 1/5000)(IWASAKI *et*

564 *al.* 2016), anti-Hop1-pT318 (rabbit, 1/5000) (IWASAKI *et al.* 2016), anti-Rec8 (rabbit,
565 1/10000) (ZHU *et al.* 2010), anti-Red1 (chicken, 1/3000) (SHINOHARA *et al.* 2008) and
566 anti-α-tubulin (YL1/2, Santa Cruz Biotechnology, 1/3000). Tubulin signals were
567 visualized using the LI-COR Bioscience system or alkaline phosphatase stain (BCIP-
568 NBT solution kit, Nacalai Tesque) on the same membrane on which other meiotic
569 proteins were detected.
570
571 **Immunoprecipitation**
572 The immunoprecipitation assay was performed as previously described with minor
573 modifications (SHINOHARA *et al.* 2008). Psy2-13Myc was immunoprecipitated by using
574 anti-Myc antibody (MC045, Nacalai Tesque) antibody which were bound to Dynabeads
575 Protein G (Thermo Fisher Scientific) from meiotic yeast cell lysate prepared using a
576 Multi-Beads shocker (YASUIKIKAI) in lysis buffer (50mM HEPES-NaOH, pH7.5,
577 150mM NaCl, 20% glycerol, 1mM Sodium orthovanadate, 60mM β-glycerophosphate,
578 0.1% Nonidet P-40, 1:100 dilution of protease inhibitor cocktail (SIGMA-Aldrich) at the
579 indicated time points in Figure 4A and 4B. Psy2-13Myc, Hop1, Red1 and Rec8 proteins
580 in the precipitates and WCEs were detected as described in the western blot section.
581
582 **Tetrad analysis**
583 Tetrad analysis was performed as described previously (CHALLA *et al.* 2019). Parental
584 haploid strains were mated for 12 h on YPAD plates at 30°C and then transferred onto
585 SPM plates. After incubation at 30°C for 48 h, tetrads were dissected onto DISS plates
586 and incubated for 48 h.
587

Acknowledgements

We are grateful to Dr. K. Matsuzaki, Dr. F. Klein, Dr. S. Gasser, and the members of the Shinohara lab for helpful discussions. We thank Ms. A. Murakami and Ms. A. Kitada for their excellent technical assistance. K.L. was supported by a Fellowship from the Institute for Protein Research, Osaka University. Special thanks to Dr. A. Shinohara for critical reading of the manuscript. This work was supported by JSPS KAKENHI (#15H05973, #19K22402) and Takeda Science Foundation, and was performed in part under the Cooperative Research Program of the Institute for Protein Research, Osaka University, CR-17-05.

598 **References**

599

600 Anderson, C. M., A. Oke, P. Yam, T. Zhuge and J. C. Fung, 2015 Reduced Crossover
601 Interference and Increased ZMM-Independent Recombination in the Absence of
602 Tel1/ATM. PLoS Genet 11: e1005478.
603 Bahler, J., J. Q. Wu, M. S. Longtine, N. G. Shah, A. McKenzie, 3rd *et al.*, 1998
604 Heterologous modules for efficient and versatile PCR-based gene targeting in
605 Schizosaccharomyces pombe. Yeast 14: 943-951.
606 Bishop, D. K., 1994 RecA homologs Dmc1 and Rad51 interact to form multiple nuclear
607 complexes prior to meiotic chromosome synapsis. Cell 79: 1081-1092.
608 Bishop, D. K., D. Park, L. Xu and N. Kleckner, 1992 DMC1: a meiosis-specific yeast
609 homolog of E. coli recA required for recombination, synaptonemal complex
610 formation, and cell cycle progression. Cell 69: 439-456.
611 Blat, Y., R. U. Protacio, N. Hunter and N. Kleckner, 2002 Physical and functional
612 interactions among basic chromosome organizational features govern early steps
613 of meiotic chiasma formation. Cell 111: 791-802.
614 Borner, G. V., A. Barot and N. Kleckner, 2008 Yeast Pch2 promotes domainal axis
615 organization, timely recombination progression, and arrest of defective
616 recombinosomes during meiosis. Proc Natl Acad Sci U S A 105: 3327-3332.
617 Borner, G. V., N. Kleckner and N. Hunter, 2004 Crossover/noncrossover differentiation,
618 synaptonemal complex formation, and regulatory surveillance at the
619 leptotene/zygotene transition of meiosis. Cell 117: 29-45.
620 Carballo, J. A., A. L. Johnson, S. G. Sedgwick and R. S. Cha, 2008 Phosphorylation of
621 the axial element protein Hop1 by Mec1/Tel1 ensures meiotic interhomolog
622 recombination. Cell 132: 758-770.
623 Challa, K., V. G. Fajish, M. Shinohara, F. Klein, S. M. Gasser *et al.*, 2019 Meiosis-
624 specific prophase-like pathway controls cleavage-independent release of cohesin
625 by Wapl phosphorylation. PLoS Genet 15: e1007851.
626 Chen, C., A. Jomaa, J. Ortega and E. E. Alani, 2014 Pch2 is a hexameric ring ATPase
627 that remodels the chromosome axis protein Hop1. Proc Natl Acad Sci U S A
628 111: E44-53.
629 Chuang, C. N., Y. H. Cheng and T. F. Wang, 2012 Mek1 stabilizes Hop1-Thr318
630 phosphorylation to promote interhomolog recombination and checkpoint
631 responses during yeast meiosis. Nucleic Acids Res 40: 11416-11427.

632 De Muyt, A., A. Pyatnitskaya, J. Andreani, L. Ranjha, C. Ramus *et al.*, 2018 A meiotic
633 XPF-ERCC1-like complex recognizes joint molecule recombination
634 intermediates to promote crossover formation. Genes Dev 32**:** 283-296.
635 Falk, J. E., A. C. Chan, E. Hoffmann and A. Hochwagen, 2010 A Mec1- and PP4-
636 dependent checkpoint couples centromere pairing to meiotic recombination. Dev
637 Cell 19**:** 599-611.
638 Farmer, S., E. J. Hong, W. K. Leung, B. Argunhan, Y. Terentyev *et al.*, 2012 Budding
639 yeast Pch2, a widely conserved meiotic protein, is involved in the initiation of
640 meiotic recombination. PLoS One 7**:** e39724.
641 Garcia, V., S. Gray, R. M. Allison, T. J. Cooper and M. J. Neale, 2015 Tel1(ATM)-
642 mediated interference suppresses clustered meiotic double-strand-break
643 formation. Nature 520**:** 114-118.
644 Hoffmann, R., S. Jung, M. Ehrmann and H. W. Hofer, 1994 The Saccharomyces
645 cerevisiae gene PPH3 encodes a protein phosphatase with properties different
646 from PPX, PP1 and PP2A. Yeast 10**:** 567-578.
647 Hollingsworth, N. M., and B. Byers, 1989 HOP1: a yeast meiotic pairing gene. Genetics
648 121**:** 445-462.
649 Hollingsworth, N. M., L. Goetsch and B. Byers, 1990 The HOP1 gene encodes a
650 meiosis-specific component of yeast chromosomes. Cell 61**:** 73-84.
651 Hustedt, N., A. Seeber, R. Sack, M. Tsai-Pflugfelder, B. Bhullar *et al.*, 2015 Yeast PP4
652 interacts with ATR homolog Ddc2-Mec1 and regulates checkpoint signaling.
653 Mol Cell 57**:** 273-289.
654 Iwasaki, D., K. Hayashihara, H. Shima, M. Higashide, M. Terasawa *et al.*, 2016 The
655 MRX Complex Ensures NHEJ Fidelity through Multiple Pathways Including
656 Xrs2-FHA-Dependent Tel1 Activation. PLoS Genet 12**:** e1005942.
657 Joshi, N., M. S. Brown, D. K. Bishop and G. V. Borner, 2015 Gradual implementation
658 of the meiotic recombination program via checkpoint pathways controlled by
659 global DSB levels. Mol Cell 57**:** 797-811.
660 Keeney, S., 2001 Mechanism and control of meiotic recombination initiation. Curr Top
661 Dev Biol 52**:** 1-53.
662 Keogh, M. C., J. A. Kim, M. Downey, J. Fillingham, D. Chowdhury *et al.*, 2006 A
663 phosphatase complex that dephosphorylates gammaH2AX regulates DNA
664 damage checkpoint recovery. Nature 439**:** 497-501.
665 Klein, F., P. Mahr, M. Galova, S. B. Buonomo, C. Michaelis *et al.*, 1999 A central role
666 for cohesins in sister chromatid cohesion, formation of axial elements, and
667 recombination during yeast meiosis. Cell 98**:** 91-103.

668 Lai, Y. J., F. M. Lin, M. J. Chuang, H. J. Shen and T. F. Wang, 2011 Genetic
669 requirements and meiotic function of phosphorylation of the yeast axial element
670 protein Red1. Mol Cell Biol 31**:** 912-923.
671 Lee, B. H., and A. Amon, 2003 Role of Polo-like kinase CDC5 in programming meiosis
672 I chromosome segregation. Science 300**:** 482-486.
673 Lo, Y. H., C. N. Chuang and T. F. Wang, 2014 Pch2 prevents Mec1/Tel1-mediated
674 Hop1 phosphorylation occurring independently of Red1 in budding yeast
675 meiosis. PLoS One 9**:** e85687.
676 Niu, H., L. Wan, B. Baumgartner, D. Schaefer, J. Loidl *et al.*, 2005 Partner choice
677 during meiosis is regulated by Hop1-promoted dimerization of Mek1. Mol Biol
678 Cell 16**:** 5804-5818.
679 Novak, J. E., P. B. Ross-Macdonald and G. S. Roeder, 2001 The budding yeast Msh4
680 protein functions in chromosome synapsis and the regulation of crossover
681 distribution. Genetics 158**:** 1013-1025.
682 O'Neill, B. M., S. J. Szyjka, E. T. Lis, A. O. Bailey, J. R. Yates, 3rd *et al.*, 2007 Pph3-
683 Psy2 is a phosphatase complex required for Rad53 dephosphorylation and
684 replication fork restart during recovery from DNA damage. Proc Natl Acad Sci
685 U S A 104**:** 9290-9295.
686 Panizza, S., M. A. Mendoza, M. Berlinger, L. Huang, A. Nicolas *et al.*, 2011 Spo11-
687 accessory proteins link double-strand break sites to the chromosome axis in
688 early meiotic recombination. Cell 146**:** 372-383.
689 Raina, V. B., and G. Vader, 2020 Homeostatic Control of Meiotic Prophase Checkpoint
690 Function by Pch2 and Hop1. Curr Biol 30**:** 4413-4424 e4415.
691 Rao, H. B. D. P., T. Sato, K. Challa, M. Shinohara and A. Shinohara, 2020
692 Phosphorylation of luminal region of the SUN-domain protein Mps3 promotes
693 nuclear envelope localization during meiosis. bioRxiv**:** 2020.2009.2015.297762.
694 Rockmill, B., and G. S. Roeder, 1988 RED1: a yeast gene required for the segregation
695 of chromosomes during the reductional division of meiosis. Proc Natl Acad Sci
696 U S A 85**:** 6057-6061.
697 San-Segundo, P. A., and G. S. Roeder, 1999 Pch2 links chromatin silencing to meiotic
698 checkpoint control. Cell 97**:** 313-324.
699 Sasanuma, H., H. Murakami, T. Fukuda, T. Shibata, A. Nicolas *et al.*, 2007 Meiotic
700 association between Spo11 regulated by Rec102, Rec104 and Rec114. Nucleic
701 Acids Res 35**:** 1119-1133.

Schwacha, A., and N. Kleckner, 1997 Interhomolog bias during meiotic recombination: meiotic functions promote a highly differentiated interhomolog-only pathway. Cell 90: 1123-1135.

Shi, Y., 2009 Serine/threonine phosphatases: mechanism through structure. Cell 139: 468-484.

Shinohara, A., S. Gasior, T. Ogawa, N. Kleckner and D. K. Bishop, 1997 Saccharomyces cerevisiae recA homologues RAD51 and DMC1 have both distinct and overlapping roles in meiotic recombination. Genes Cells 2: 615-629.

Shinohara, M., D. K. Bishop and A. Shinohara, 2019 Distinct Functions in Regulation of Meiotic Crossovers for DNA Damage Response Clamp Loader Rad24(Rad17) and Mec1(ATR) Kinase. Genetics 213: 1255-1269.

Shinohara, M., S. L. Gasior, D. K. Bishop and A. Shinohara, 2000 Tid1/Rdh54 promotes colocalization of rad51 and dmc1 during meiotic recombination. Proc Natl Acad Sci U S A 97: 10814-10819.

Shinohara, M., K. Hayashihara, J. T. Grubb, D. K. Bishop and A. Shinohara, 2015 DNA damage response clamp 9-1-1 promotes assembly of ZMM proteins for formation of crossovers and synaptonemal complex. J Cell Sci 128: 1494-1506.

Shinohara, M., S. D. Oh, N. Hunter and A. Shinohara, 2008 Crossover assurance and crossover interference are distinctly regulated by the ZMM proteins during yeast meiosis. Nat Genet 40: 299-309.

Shinohara, M., K. Sakai, T. Ogawa and A. Shinohara, 2003 The mitotic DNA damage checkpoint proteins Rad17 and Rad24 are required for repair of double-strand breaks during meiosis in yeast. Genetics 164: 855-865.

Shinohara, M., and A. Shinohara, 2013 Multiple pathways suppress non-allelic homologous recombination during meiosis in Saccharomyces cerevisiae. PLoS One 8: e63144.

Storlazzi, A., L. Xu, A. Schwacha and N. Kleckner, 1996 Synaptonemal complex (SC) component Zip1 plays a role in meiotic recombination independent of SC polymerization along the chromosomes. Proc Natl Acad Sci U S A 93: 9043-9048.

Subramanian, V. V., A. J. MacQueen, G. Vader, M. Shinohara, A. Sanchez *et al.*, 2016 Chromosome Synapsis Alleviates Mek1-Dependent Suppression of Meiotic DNA Repair. PLoS Biol 14: e1002369.

Sun, X., L. Huang, T. E. Markowitz, H. G. Blitzblau, D. Chen *et al.*, 2015 Transcription dynamically patterns the meiotic chromosome-axis interface. Elife 4.

737 Sym, M., J. A. Engebrecht and G. S. Roeder, 1993 ZIP1 is a synaptonemal complex
738 protein required for meiotic chromosome synapsis. Cell 72: 365-378.
739 Tsubouchi, T., and G. S. Roeder, 2005 A synaptonemal complex protein promotes
740 homology-independent centromere coupling. Science 308: 870-873.
741 Wan, L., C. Zhang, K. M. Shokat and N. M. Hollingsworth, 2006 Chemical inactivation
742 of cdc7 kinase in budding yeast results in a reversible arrest that allows efficient
743 cell synchronization prior to meiotic recombination. Genetics 174: 1767-1774.
744 West, A. M. V., E. A. Komives and K. D. Corbett, 2018 Conformational dynamics of
745 the Hop1 HORMA domain reveal a common mechanism with the spindle
746 checkpoint protein Mad2. Nucleic Acids Res 46: 279-292.
747 Zhang, L., K. P. Kim, N. E. Kleckner and A. Storlazzi, 2011 Meiotic double-strand
748 breaks occur once per pair of (sister) chromatids and, via Mec1/ATR and
749 Tel1/ATM, once per quartet of chromatids. Proc Natl Acad Sci U S A 108:
750 20036-20041.
751 Zhu, Z., S. Mori, H. Oshiumi, K. Matsuzaki, M. Shinohara *et al.*, 2010 Cyclin-
752 dependent kinase promotes formation of the synaptonemal complex in yeast
753 meiosis. Genes Cells 15: 1036-1050.

754

755

756 **Figure legends**

757

758 **Figure1. PP4 dephosphorylation activity is required for proper meiotic**

759 **recombination.**

760 (A) Schematic of the functional domain structure of yeast Pph3 (*sc*Pph3) protein.

761 Amino acid sequences contributing to phosphate binding and metal

762 coordination are shown in pale blue and red, respectively. The position of the

763 *pph3-H112N* and the substitution of histidine 112 with asparagine is shown.

764 (B) Localization of Psy2-13Myc was analyzed in *PPH3* (MSY6198/6190) and the

765 *pph3-H112N* (MSY6242/6244) background by immunostaining with anti-Myc

766 antibody (green). Representative images at 6h in meiosis are shown**.** Scale bar

767 indicates 2 μm.

768 (C) Schematics of the *HIS4-LEU2* recombination hotspot. Diagnostic P: *Pst*I, X:

769 *Xho*I, B: *Bam*HI and M: *Mlu*I restriction sites are shown. The size of meiotic

770 DSBs (DSB I, DSB II), and parental (Pa), and heteroduplexes (HDs) that are

771 associated with COs (HD2 and HD3) or NCOs (HD1 and HD4), Parental (Pa1

772 and Pa2) and the positions of detectable probes 291 and 155 are shown.

773 (D) Representative Southern blotting of DSB detection in wild type (black,

774 NKY1303/1543), *pph3*Δ (red, MSY5632/MSY5634), *pph3-H112N* (blue,

775 MSY6219/6220), p*CLB2-MEC1 tel1*Δ (purple, MSY5544/5546) and p*CLB2-*

776 *MEC1 tel1*Δ *pph3*Δ (orange, MSY5760/5762) using probe 291. The graph

777 shows the mean and standard error of the quantified DSB I signals from more

778 than three times trials.

779 (E) Representative Southern blotting of HD-associated COs and NCOs formed at

780 the *HIS4-LEU2* hotspot using probe155. The upper graph shows the mean and
781 standard error of the quantified HD-associated COs (HD2 and HD3). The lower
782 graph shows the mean and standard error of the quantified HD-associated
783 NCOs (HD1 and HD4) of wild type, *pph3*Δ, and *pph3-H112N.*
784 (F) Representative immunostaining images of Rad51 (green) at 3 h on meiotic
785 nuclear spreads in wild type (NKY1303/1543), *pph3*Δ (MSY5632/MSY5634),
786 and *pph3-H112N* (MSY6219/6220). Scale bar indicates 2 μm. The dot plot
787 graph shows the distribution of the number of Rad51 foci in each Rad51 focus
788 positive nucleus at the indicated time points in wild type (black, NKY1303/1543),
789 *pph3*Δ (red, MSY5632/MSY5634), and *pph3-H112N* (blue, MSY6219/6220).
790 The data are presented as the medians and 95% confidence interval. Asterisks
791 indicate statistically significant differences between the indicated strains
792 determined using the Mann-Whitney U-test (* $P<0.05$, ** $P<0.01$, **** $P<0.0001$)
793 using Prism9 software.
794
795 **Figure 2. Hop1 assembly is delayed in the *pph3* mutant in early prophase-I.**
796 (A) Graphic depiction of the kinetics of Hop1 focus (upper) and Hop1-pT318 focus
797 (lower) assembly on meiotic nuclear spreads in the indicated strains, wild type
798 (black, NKY1303/1543), *pph3*Δ (red, MSY5632/MSY5634), *pph3-H112N* (blue,
799 MSY6219/6220), p*CLB2-MEC1 tel1*Δ (purple, MSY5544/5546) and p*CLB2-*
800 *MEC1 tel1*Δ *pph3*Δ (orange, MSY5760/5762). More than 100 cells were
801 analyzed in each time point. Error bars show the mean ± standard deviation
802 from more than three times trials.
803 (B) Representative cytological immunostaining images of Hop1 (green) and Hop1-

804 pT318 (red) on meiotic nuclear spreads at 3 h in wild type (NKY1303/1543),
805 *pph3*Δ (MSY5632/MSY5634), and *pph3-H112N* (MSY6219/6220). Scale bar
806 indicates 2 μm.
807 (C) Representative western blot images of phosphorylation of histone H2A (γH2A,
808 red) and α-tubulin expression (green) at the indicated time point during meiosis
809 (upper panel). Expression of Hop1 (green, top), phosphorylation of Hop1 at
810 T318 (Hop1-pT318, red, middle), merged images of Hop1 and Hop1-pT318,
811 and α-tubulin expression (bottom) at the indicated time points during meiosis. M
812 denotes molecular weight markers.
813 (D) Grapic depiction of the average of the relative Hop1 protein signals from
814 western blot at each time point. The numerical values are shown as a
815 percentage of the peak amount of signal in the wild type. Error bars show the
816 mean and ± standard deviation from two independent trials.
817
818 **Figure 3. Rec8 expression is normal in the *pph3* mutant in early prophase I.**
819 (A) Representative cytological immunostaining images of Rec8 (green) and Red1
820 (red) on meiotic nuclear spreads at 3 h in wild type (NKY1303/1543), *pph3*Δ
821 (MSY5632/MSY5634), *pph3-H112N* (MSY6219/6220). wild type
822 (NKY1303/1543), *pch2*Δ (MSY6446/6448), *pph3*Δ (MSY5632/MSY5634) and
823 *pph3*Δ *pch2*Δ (MSY6417/6419)
824 (B) Graphs show the kinetics of Rec8 (upper) and Red1 (lower) focus assembly on
825 meiotic nuclear spreads in the indicated strains, wild type (black,
826 NKY1303/1543), *pph3*Δ (red, MSY5632/MSY5634), and *pph3-H112N* (blue,
827 MSY6219/6220). More than 100 cells were analyzed at each time point. Error

828 bars show the mean ± standard deviation from more than three times trials.

829 (C) Representative western blot images of expression of Rec8 (upper) and Red1
830 (lower) with α-tubulin expression images as internal controls at the indicated
831 time points during meiosis. M denotes molecular weight markers. Asterisks
832 indicate non-specific protein signals.

833

834 **Figure 4. PP4 interacts with Hop1 during meiosis.**

835 (A) Immunoprecipitation (IP) analysis of Psy2-13Myc from *PPH3* (non-tag,
836 NKY1303/1543), *PPH3* (*PSY2-13MYC*, MSY6188/6190), *pph3-H112N*
837 (MSY6219/6220) and *pph3-H112N* (*PSY2-13MYC*, MSY6242/6244) cells at the
838 indicated time points during meiosis. Immunoprecipitation products were probed
839 with anti-Myc and anti-Hop1 antibodies.

840 (B) Immunoprecipitation (IP) analysis of Psy2-13Myc from *PPH3* (non-tag,
841 NKY1303/1543) and *PPH3* (*PSY2-13MYC*, MSY6188/6190) cells at the
842 indicated time points during meiosis. Whole cell extracts and
843 immunoprecipitation products were probed with anti-Myc, anti-Hop1, anti-Red1
844 and anti-Rec8 antibodies.

845 (C) Tetrad analysis of spore viability in wild type (NKY1303/1543), *pph3*Δ
846 (MSY5632/MSY5634), *pch2*Δ (MSY6446/6448) and *pph3*Δ *pch2*Δ
847 (MSY6417/6419). The graphs show the fraction of tetrads containing 0-, 1-, 2-,
848 3- and 4-viable spores. The overall spore viability is shown in parentheses. n:
849 number of asci analyzed.

850 (D) Graphic depiction of the kinetics of Hop1 (left) and Hop1-pT318 (right) focus
851 assembly on meiotic nuclear spreads in the indicated strains, wild type (black,

852 NKY1303/1543), *pch2*Δ (gray, MSY6446/6448), *pph3*Δ (red,
853 MSY5632/MSY5634) and *pph3*Δ *pch2*Δ (orange, MSY6417/6419). More than
854 100 cells were analyzed at each time point. Error bars show the mean ±
855 standard deviation from more than three times trials.
856 (E) Representative cytological immunostaining images of Hop1 (green) and Hop1-
857 pT318 (red) on meiotic nuclear spreads at 3 h (left panel) and 6 h (right panel)
858 in wild type (NKY1303/1543), *pch2*Δ (MSY6446/6448), *pph3*Δ
859 (MSY5632/MSY5634) and *pph3*Δ *pch2*Δ (MSY6417/6419). Scale bar indicates
860 2 μm.
861
862 **Figure 5. *pch2*Δ does not completely suppress the defect in Hop1 assembly**
863 **of *pph3*Δ.**
864 (A) Zip1 and Hop1 elongation was analyzed in wild type (NKY1303/1543), *pch2*Δ
865 (MSY6446/6448), *pph3*Δ (MSY5632/MSY5634), and *pph3*Δ *pch2*Δ
866 (MSY6417/6419) via immunostaining at each time point. The graphs show the
867 percentages of each class of Zip1 morphologies; linear (dark gray, pachytene),
868 partial (pale gray, zygotene) and dotty (black, leptotene). Error bars show the
869 mean ± standard deviation from more than three trials. More than 100 cells at
870 each time point were analyzed.
871 (B) Representative cytological immunostaining images of Hop1 (green) and Zip1
872 (red) on pachytene-phase nuclear spreads at 4 h in wild type (NKY1303/1543),
873 and 6 h in the *pch2*Δ (MSY6446/6448), *pph3*Δ (MSY5632/MSY5634) and
874 *pph3*Δ *pch2*Δ (MSY6417/6419). Scale bar indicates 2 μm.
875 (C) The dot plot graph of the distribution of the number of linearized Hop1 signals in

876 each pachytene stage nucleus in *pch2*Δ (N = 112) and *pph3*Δ *pch2*Δ (N = 109)
877 at 6 h during meiosis from three independent trials. Error bars show the mean
878 with 95% confidence interval. Statistically significant differences between the
879 *pch2*Δ and *pph3*Δ *pch2*Δ were determined using the Mann-Whitney U-test (****
880 *P*<0.0001) using Prism9 software.
881 (D) The dot plot graph of the distribution of lengths of linearized Hop1 signal of
882 pachytene stage nucleus in *pch2*Δ (gray, N = 718) and *pph3*Δ *pch2*Δ (orange,
883 N = 780) at 6 h in meiosis from three independent trials. Error bars show the
884 mean with 95% confidence interval. Statistically significant differences between
885 the *pch2*Δ and *pph3*Δ *pch2*Δ were determined using the Mann-Whitney U-test
886 (ns; not significant) using Prism9 software.
887 (E) Representative cytological immunostaining images of Rec8 (green) and Red1
888 (red) on pachytene-stage nuclear spreads in wild type (3 h, NKY1303/1543),
889 *pch2*Δ (6 h, MSY6446/6448), *pph3*Δ (6 h, MSY5632/MSY5634) and *pph3*Δ
890 *pch2*Δ (6 h, MSY6417/6419). Scale bar indicates 2 μm.
891 (F) Representative western blot images of expression of Hop1 expression (green)
892 and phosphorylation of Hop1 at pT318 (Hop1-pT318, red) and α-tubulin
893 expression (bottom) at the indicated time points during meiosis. M denotes
894 molecular weight markers.
895 (G) Meiosis progression in wild type (black, NKY1303/1543), *pch2*Δ (gray,
896 MSY6446/6448), *pph3*Δ (red, MSY5632/MSY5634) and *pph3*Δ *pch2*Δ (orange,
897 MSY6417/6419) mutants are shown. Frequencies of nuclei with more than two
898 DAPI-staining bodies at each time point are plotted. More than 100 cells were
899 analyzed at each time point. Error bars show the means and standard deviation

900 from two independent trials.

901

902 **Figure 6. Model for PP4 involvement in Hop1 loading onto meiotic chromatin.**

903 PP4 plays multiple roles during meiotic prophase. First, PP4 promotes Hop1

904 loading in the early phase of meiotic prophase in a Mec1/Tel1-independent manner.

905 Until the chromatin loading, Hop1 exists in an inactive form, which might prevent

906 miosis progression. After meiotic DSB formation, Hop1 is phosphorylated at the

907 DSB site by Tel1/Mec1, and PP4 is involved in dephosphorylation of the

908 phosphorylated Hop1. Meiotic recombination promotes homolog synapsis by

909 exchanging Hop1 to Zip1 through the function of AAA+ Pch2 function.

910

911

912 Supplemental figure 1. **Supplemental data for Figure 1.**

913 (A) Representative western blot images showing Psy2-13myc and α-tubulin

914 expression at the indicated time points during meiosis in wild type (non-tag,

915 NKY1303/1543), *pph3*Δ (non-tag, MSY5632/5634), PSY2-13myc

916 (MSY6188/6190), *pph3-H112N* (non-tag, MSY6219/6220) and *PSY2-13MYC*

917 *pph3-H112N* (MSY6242/6244).

918 (B) Meiosis progression in wild type (NKY1303/1543), *pph3*Δ (MSY5632/5634) and

919 *pph3-H112N* (MSY6219/6220) mutants. Frequencies of nuclei with more than

920 two DAPI-stained bodies are plotted.

921 (C) The graph of the kinetics of Rad51 focus assembly on meiotic nuclear spreads

922 in wild type (black, NKY1303/1543), *pph3*Δ (red, MSY5632/MSY5634), and

923 *pph3-H112N* (blue, MSY6219/6220). More than 100 cells were analyzed at

924 each time point. Error bars show the mean ± standard deviation from more than
925 three times trials.
926
927 Supplemental Figure 2. **Supplemental data presentation for Figure 4.**
928 (A) Whole membrane images of western blot of immunoprecipitates (IP) are
929 shown in Figure 4A and western blot of whole cell extracts (WCEs) before the
930 immunoprecipitation.
931 (B) Whole membrane images of western blot of immunoprecipitates (IP) and
932 whole cell extracts (WCEs) exhibited in Figure 4B,
933

Li *et al* Figure 1

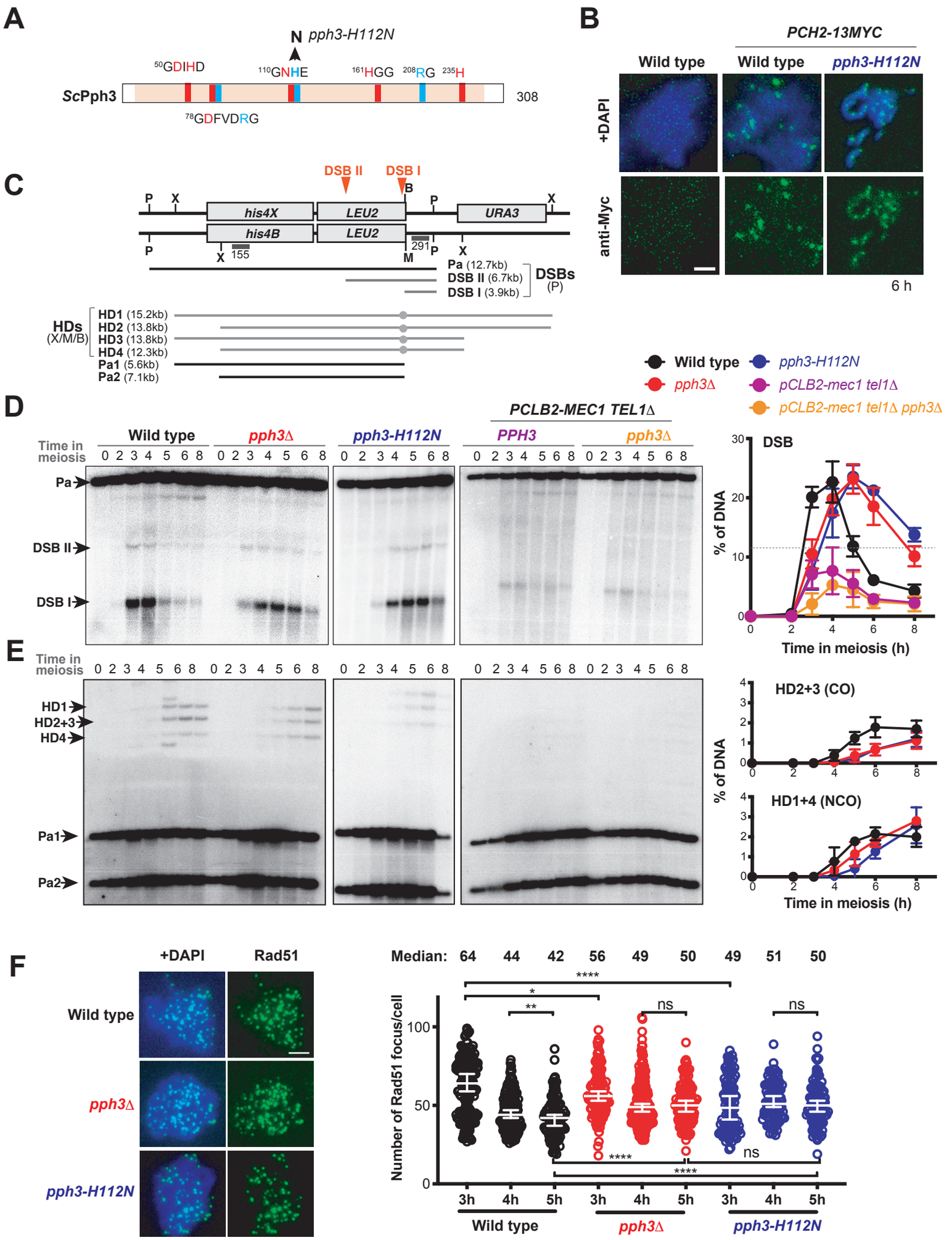

Li *et al* Figure 2

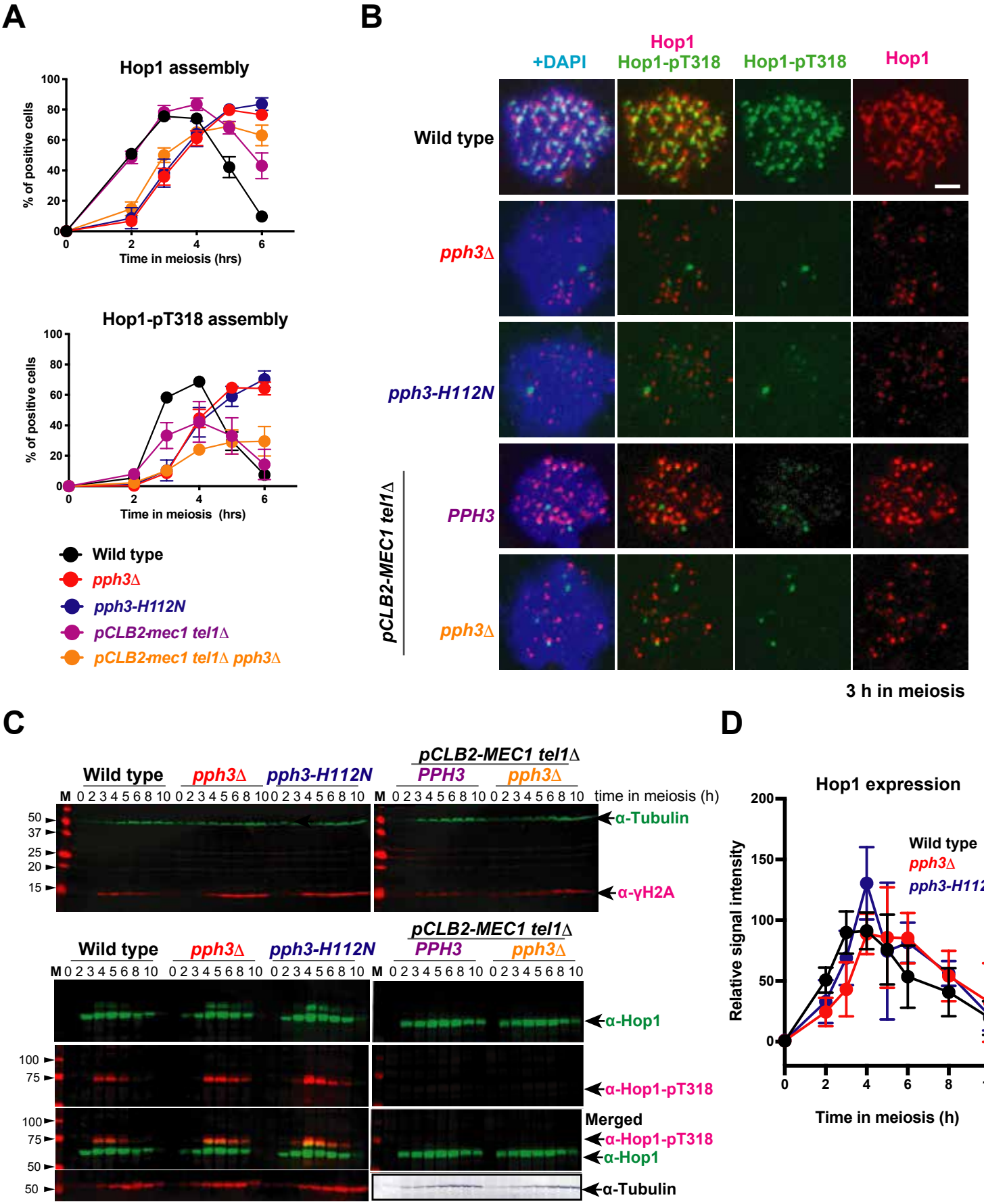

Li *et al* Figure 3

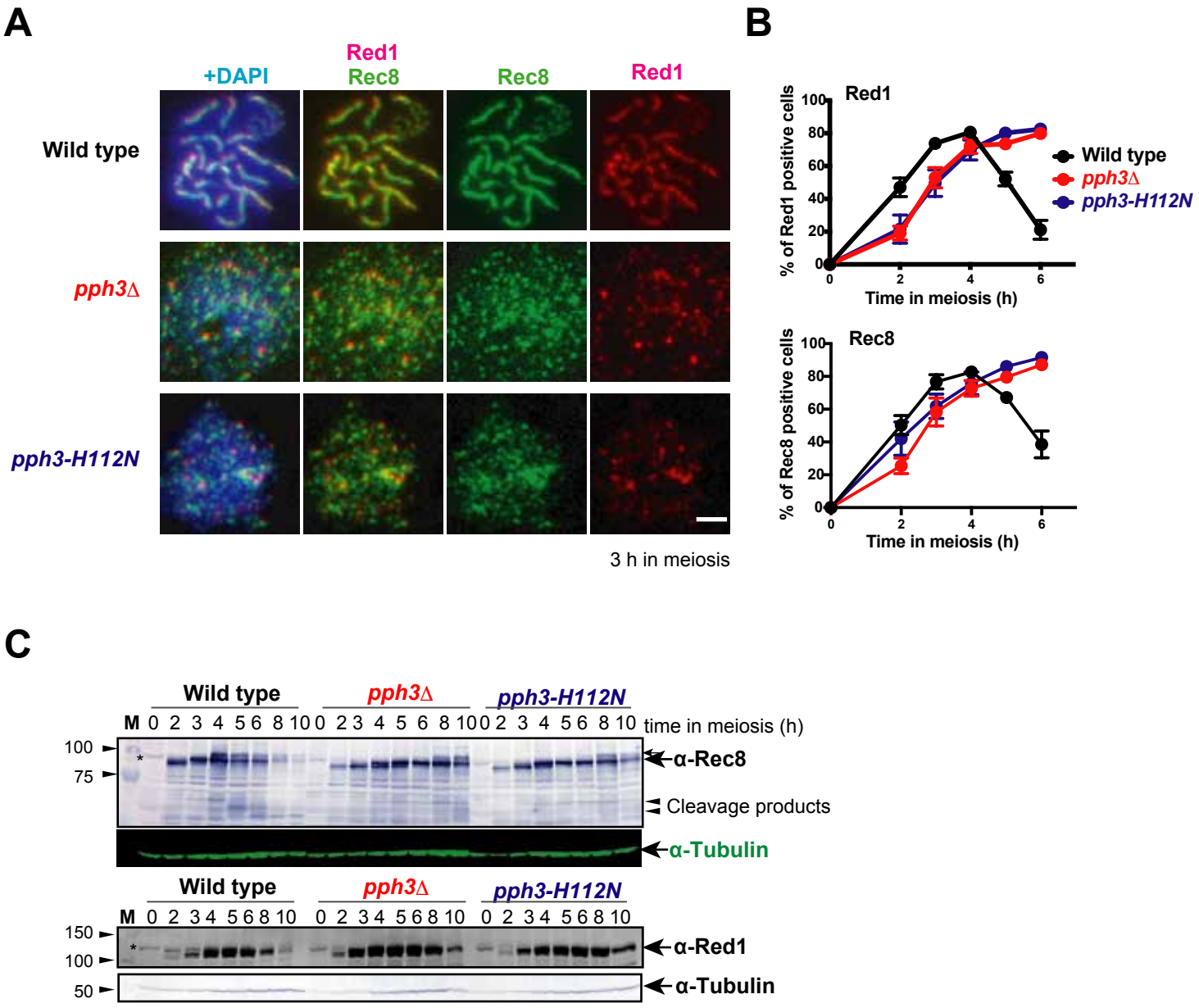

Li *et al* Figure 4

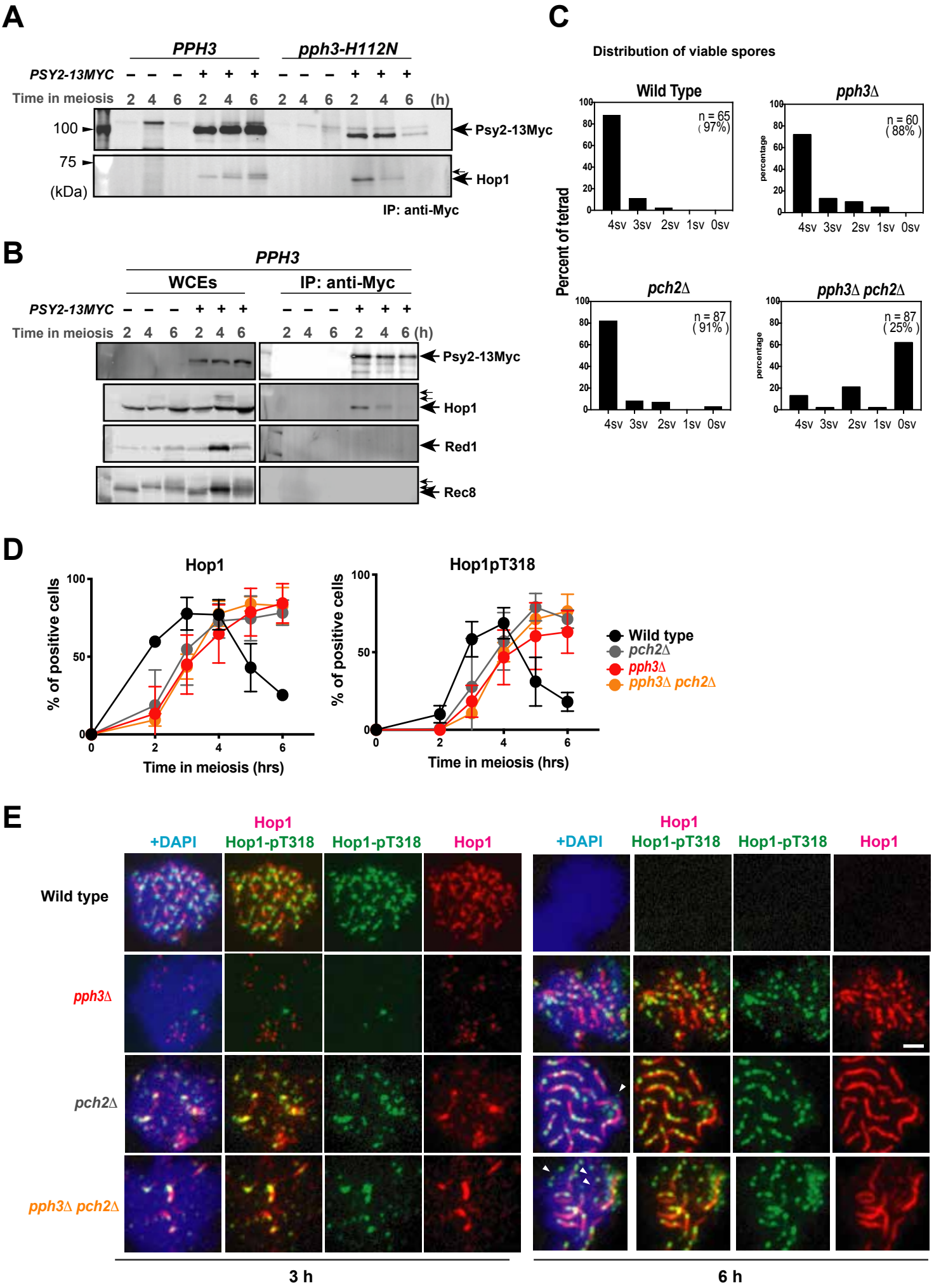

Li *et al* Figure 5

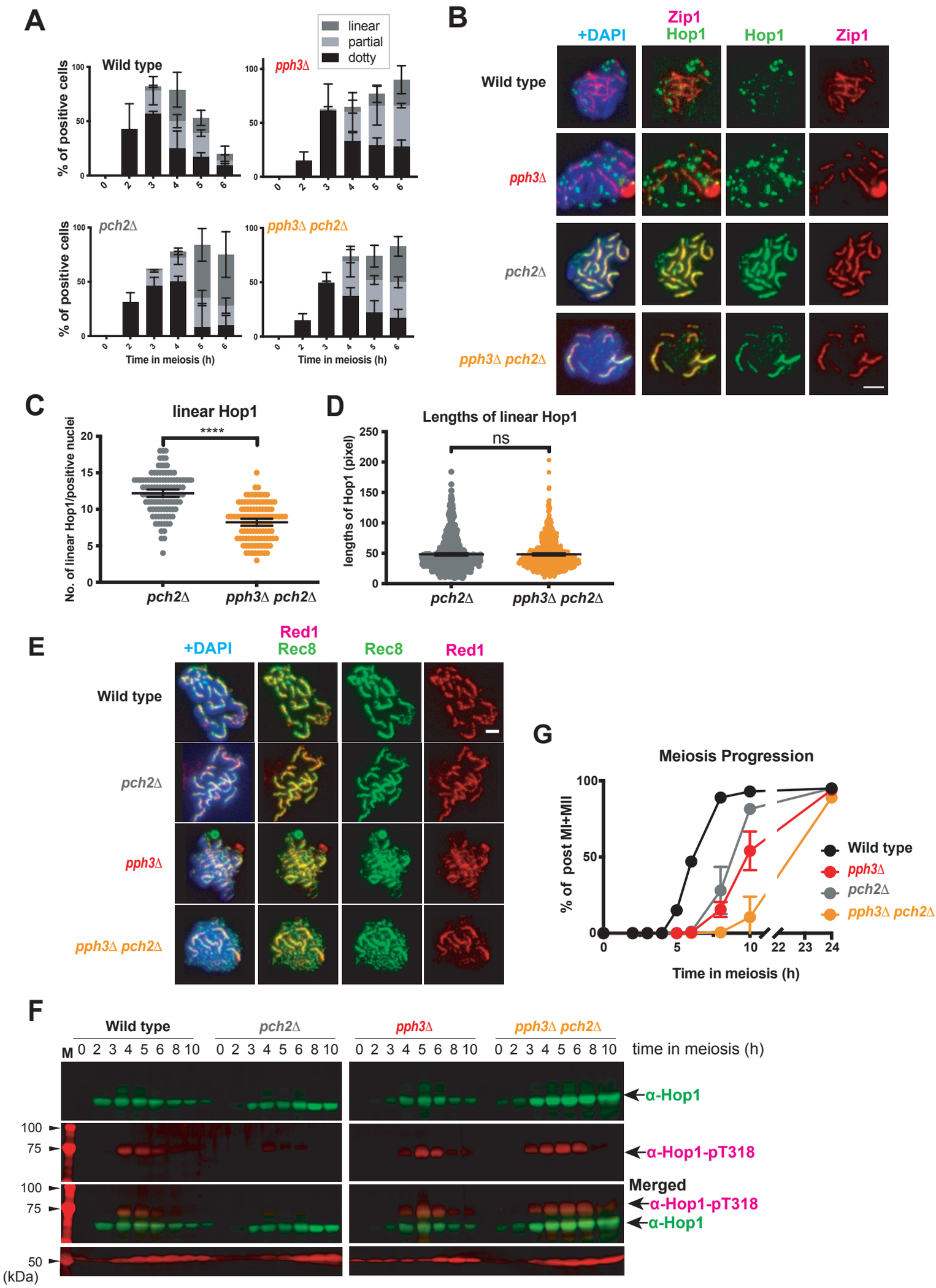

Li *et al*, Figure 6

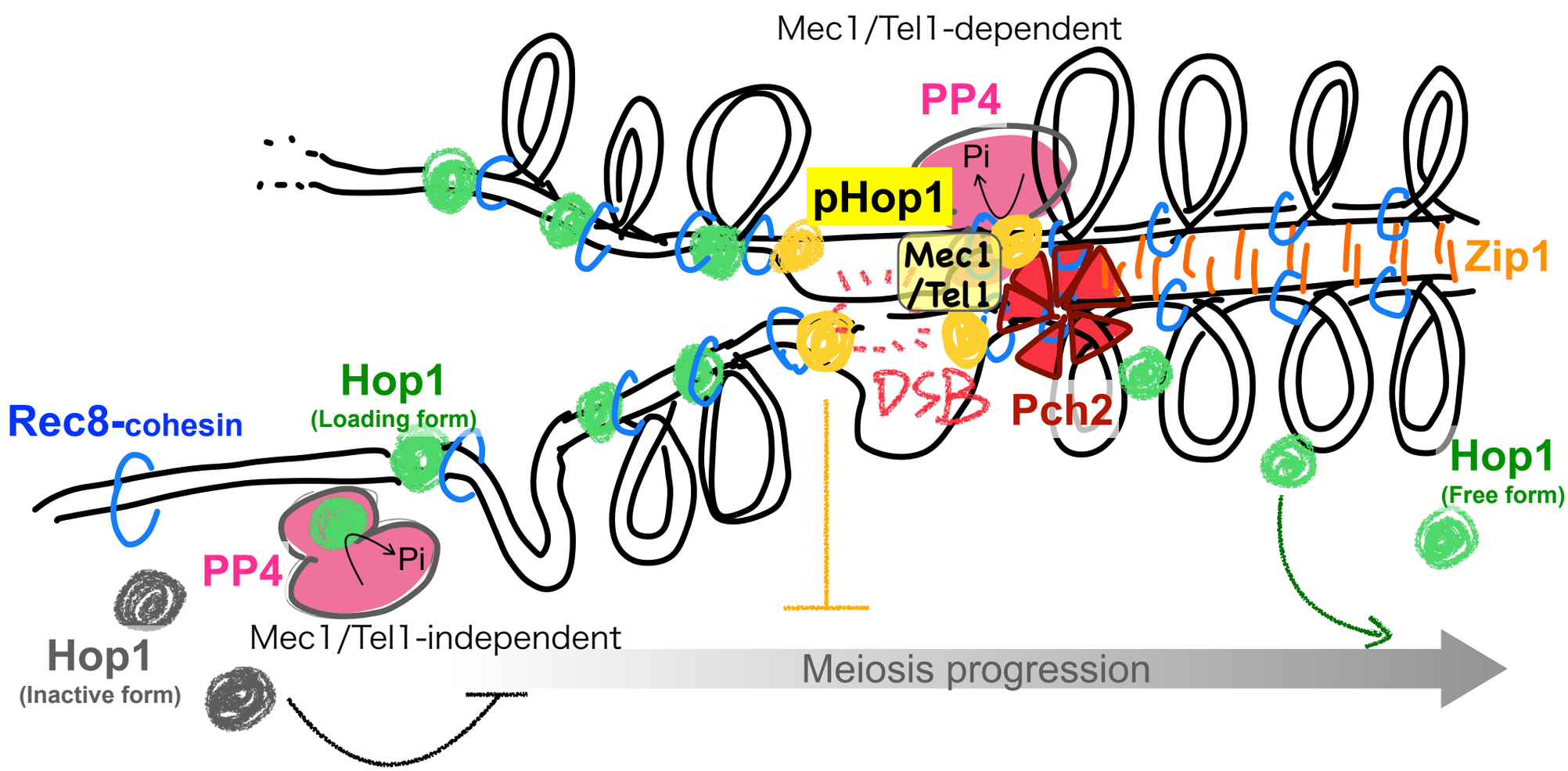

Supplemental Table-1 Strain list

Strain	Genotype	Reference
NKY1303	*MAT*a, *ho::LYS2, lys2, ura3, leu2::hisG, his4B-LEU2(Mlu*I*), arg4 bgl*	(STORLAZZI *et al.* 1996)
NKY1543	*MATa, ho::LYS2, lys2, ura3, leu2::hisG, his4X-LEU2(Bam*HI*)-URA3, arg4-nsp*	(STORLAZZI *et al.* 1996)
MSY5632	NKY1303 with *pph3::Hyg*^{R}	This study
MSY5634	NKY1543 with *pph3::Hyg*^{R}	This study
MSY6219	NKY1303 with *pph3-H112N::MluI*	This study
MSY6220	NKY1543 with *pph3-H112N::MluI*	This study
MSY6198	NKY1303 with *PSY2-13MYC::TRP1*	This study
MSY6190	NKY1543 with *PSY2-13MYC::TRP1*	This study
MSY6242	NKY1303 with *PSY2-13MYC::TRP1, pph3-H112N::MluI*	This study
MSY6244	NKY1543 with *PSY2-13MYC::TRP1, pph3-H112N::MluI*	This study
MSY5544	NKY1303 with *pCLB2-MEC1, tel1::TRP1*	This study
MSY5546	NKY1543 with *pCLB2-MEC1, tel1::TRP1*	This study
MSY5760	NKY1303 with *pCLB2-MEC1, tel1::TRP1, pph3::Hyg*^{R}	This study
MSY5762	NKY1543 with *pCLB2-MEC1, tel1::TRP1, pph3::Hyg*^{R}	This study
MSY6446	NKY1303 with *pch2::TRP1*	This study
MSY6448	NKY1543 with *pch2::TRP1*	This study
MSY6417	NKY1303 with *pph3::Hyg*^{R}*, pch2::TRP1*	This study
MSY6519	NKY1543 with *pph3::Hyg*^{R}*, pch2::TRP1*	This study

Storlazzi, A., L. Xu, A. Schwacha and N. Kleckner, 1996 Synaptonemal complex (SC) component Zip1 plays a role in meiotic recombination independent of SC polymerization along the chromosomes. Proc Natl Acad Sci U S A 93: 9043-9048.

Supplemental Figure 1, Li *et al*

A

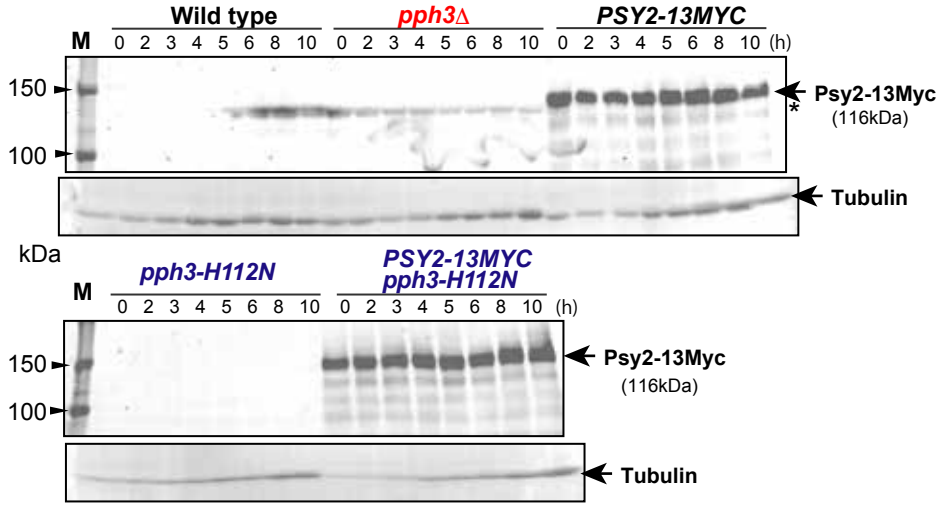

B

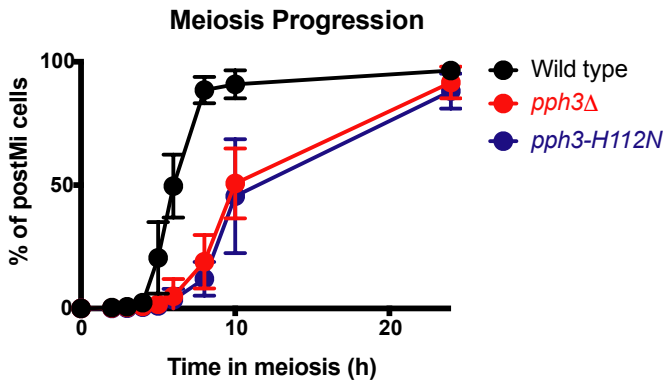

C

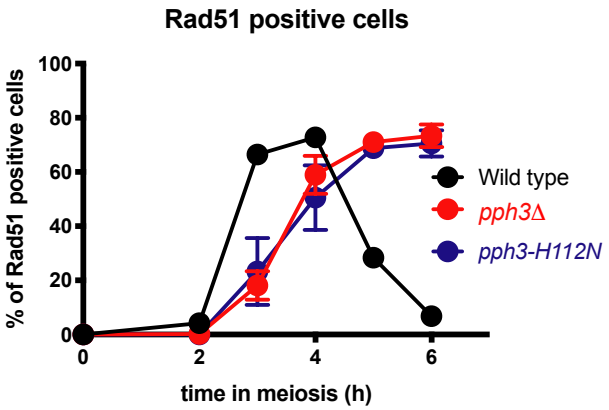
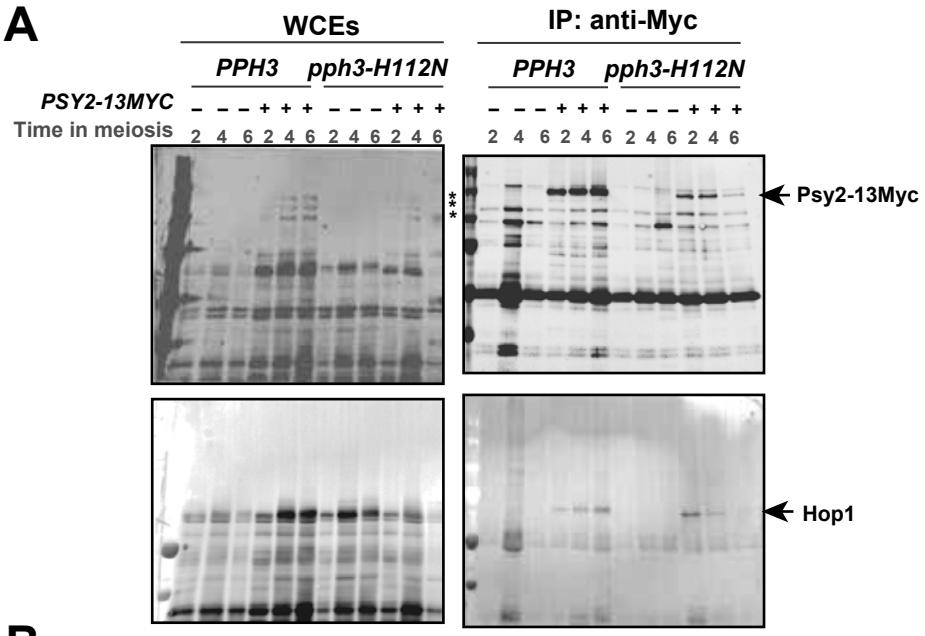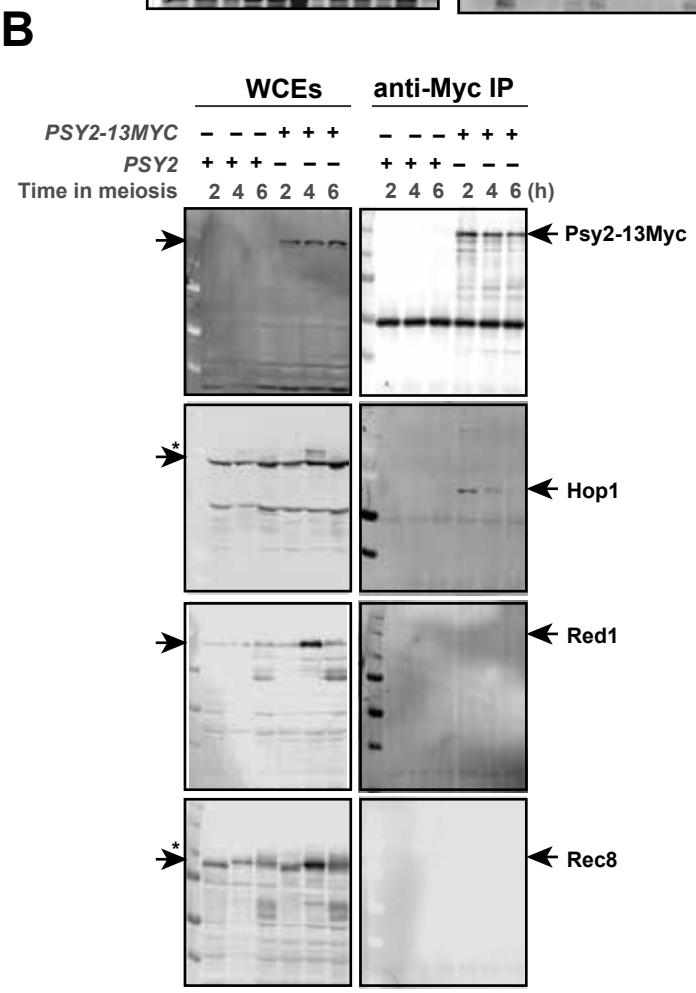
Supplemental Figure 2, Li *et al*